ELSEVIER

Advances in Colloid and Interface Science 111 (2004) 3–27

ADVANCES IN COLLOID AND INTERFACE SCIENCE

www.elsevier.com/locate/cis

# Surfactant solutions and porous substrates: spreading and imbibition

Victor M. Starov*

*Department of Chemical Engineering, Loughborough University, Loughborough, LE11 3TU, UK*

Available online 27 September 2004

**Abstract**

In Section 1, spreading of small liquid drops over thin dry porous layers is investigated from both theoretical and experimental points of view [V.M. Starov, S.R. Kosvintsev, V.D. Sobolev, M.G. Velarde, S.A. Zhdanov, J. Colloid Interface Sci. 252 (2002) 397]. Drop motion over a porous layer is caused by an interplay of two processes: (a) the spreading of the drop over already saturated parts of the porous layer, which results in an expanding of the drop base, and (b) the imbibition of the liquid from the drop into the porous substrate, which results in a shrinkage of the drop base and an expanding of the wetted region inside the porous layer. As a result of these two competing processes, the radius of the drop goes through a maximum value over time. A system of two differential equations has been derived to describe the evolution with time of radii of both the drop base and the wetted region inside the porous layer. This system includes two parameters, one accounts for the effective lubrication coefficient of the liquid over the wetted porous substrate, and the other is a combination of permeability and effective capillary pressure inside the porous layer. Two additional experiments were used for an independent determination of these two parameters. The system of differential equations does not include any fitting parameter after these two parameters are determined. Experiments were carried out on the spreading of silicone oil drops over various dry microfiltration membranes (permeable in both normal and tangential directions). The time evolution of the radii of both the drop base and the wetted region inside the porous layer were monitored. All experimental data fell on two universal curves if appropriate scales are used with a plot of the dimensionless radii of the drop base and of the wetted region inside the porous layer on dimensionless time. The predicted theoretical relationships are two universal curves accounting quite satisfactory for the experimental data. According to theory predictions [1]: (i) the dynamic contact angle dependence on the same dimensionless time as before should be a universal function, and (ii) the dynamic contact angle should change rapidly over an initial short stage of spreading and should remain a constant value over the duration of the rest of the spreading process. The constancy of the contact angle on this stage has nothing to do with hysteresis of the contact angle: there is no hysteresis in the system under investigation. These conclusions again are in good agreement with experimental observations [V.M. Starov, S.R. Kosvintsev, V.D. Sobolev, M.G. Velarde, S.A. Zhdanov, J. Colloid Interface Sci. 252 (2002) 397].

In Section 2, experimental investigations are reviewed on the spreading of small drops of aqueous SDS solutions over dry thin porous substrates (nitrocellulose membranes) in the case of partial wetting [S. Zhdanov, V. Starov, V. Sobolev, M. Velarde, Spreading of aqueous SDS solutions over nitrocellulose membranes. J. Colloid Interface Sci. 264 (2003) 481-489]. The time evolution was monitored of the radii of both the drop base and the wetted area inside the porous substrate. The total duration of the spreading process was subdivided into three stagesthe *first stage*: the drop base expands until the maximum value of the drop base is reached; the contact angle rapidly decreases during this stage; the *second stage*: the radius of the drop base remains constant and the contact angle decreases linearly with time; the *third stage*: the drop base shrinks and the contact angle remains constant. The wetted area inside the porous substrate expends during the whole spreading process. Appropriate scales were used with a plot of the dimensionless radii of the drop base, of the wetted area inside the porous substrate, and the dynamic contact angle on the dimensionless time. Experimental data showed [S. Zhdanov, V. Starov, V. Sobolev, M. Velarde, Spreading of aqueous SDS solutions over nitrocellulose membranes. J. Colloid Interface Sci. 264 (2003) 481-489]: the overall time of the spreading of drops of SDS solution over dry thin porous substrates decreases with the increase of surfactant concentration; the difference between advancing and hydrodynamic receding contact angles decreases with the surfactant concentration increase; the constancy of the contact angle during the third stage of spreading has nothing to do with the hysteresis of contact angle, but determined by the hydrodynamic reasons. It is shown using independent spreading experiments of the same drops on nonporous nitrocellulose substrate that the static receding contact angle is equal to zero, which supports the conclusion on the hydrodynamic nature of the hydrodynamic receding contact angle on porous substrates.

* Tel.: +44 1509 222508; fax: +44 01509 223 923.
*E-mail address:* V.M.Starov@lboro.ac.uk.


doi:10.1016/j.cis.2004.07.007

In Section 3, a theory is developed to describe a spontaneous imbibition of surfactant solutions into hydrophobic capillaries, which takes into account the micelle disintegration and the concentration decreasing close to the moving meniscus as a result of adsorption, as well as the surface diffusion of surfactant molecules [N.V. Churaev, G.A. Martynov, V.M. Starov, Z.M. Zorin, Colloid Polym. Sci. 259 (1981) 747]. The theory predictions are in good agreement with the experimental investigations on the spontaneous imbibition of the nonionic aqueous surfactant solution, Syntamide-5, into hydrophobized quartz capillaries. A theory of the spontaneous capillary rise of surfactant solutions in hydrophobic capillaries is presented, which connects the experimental observations with the adsorption of surfactant molecules in front of the moving meniscus on the bare hydrophobic interface [V.J. Starov, Colloid Interface Sci. 270 (2003)].

In Section 4, capillary imbibition of aqueous surfactant solutions into dry porous substrates is investigated from both theoretical and experimental points of view in the case of partial wetting [V. Straov, S. Zhdanov, M. Velarde, J. Colloid Interface Sci. 273 (2004) 589]. Cylindrical capillaries are used as a model of porous media for theoretical treatment of the problem. It is shown that if an averaged pore size of the porous medium is below a critical value, then the permeability of the porous medium is not influenced by the presence of surfactants at any concentration: the imbibition front moves exactly in the same way as in the case of the imbibition of the pure water. The critical radius is determined by the adsorption of the surfactant molecules on the inner surface of the pores. If an averaged pore size is bigger than the critical value, then the permeability increases with surfactant concentration. These theoretical conclusions are in agreement with experimental observations.

In Section 5, the spreading of surfactant solutions over hydrophobic surfaces is considered from both theoretical and experimental points of view [V.M. Starov, S.R. Kosvintsev, M.G. Velarde, J. Colloid Interface Sci. 227 (2000) 185]. Water droplets do not wet a virgin solid hydrophobic substrate. It is shown that the transfer of surfactant molecules from the water droplet onto the hydrophobic surface changes the wetting characteristics in front of the drop on the three-phase contact line. The surfactant molecules increase the solidvapor interfacial tension and hydrophilise the initially hydrophobic solid substrate just in front of the spreading drop. This process causes water drops to spread over time. The time of evolution of the spreading of a water droplet is predicted and compared with experimental observations. The assumption that surfactant transfer from the drop surface onto the solid hydrophobic substrate controls the rate of spreading is confirmed by experimental observations.

In Section 6, the process of the spontaneous spreading of a droplet of a polar liquid over solid substrate is analyzed in the case when amphiphilic molecules (or their amphiphilic fragments) of the substrate surface layer are capable of overturning, resulting in a partial hydrophilisation of the surface [V.M. Starov, V.M. Rudoy, V.I. Ivanov, Colloid J. (Russian Academy of Sciences English Transaction) 61 (3) (1999) 374]. Such a situation may take place, for example, during contact of an aqueous droplet with the surface of a polymer whose macromolecules have hydrophilic side groups capable of rotating around the backbone and during the wetting of polymers containing surface-active additives or LangmuirBlodgett films composed of amphiphilic molecules. It was shown that droplet spreading is possible only if the lateral interaction between neighbouring amphiphilic molecules (or groups) takes place. This interaction results in the tangential transfer of the overturning state to some distance in front of the advancing three-phase contact line making it partially hydrophilic. The quantitative theory describing the kinetics of droplet spreading is developed with allowance for this mechanism of self-organization of the surface layer of a substrate in the contact with a droplet.



*Keywords:* Surfactant solutions; Porous substrates; Imbibition

**Contents**

## 1. Spreading of liquid drops over dry porous substrates in the case of complete wetting: universal behaviour

In this section, we take up the problem in the case of complete wetting when a drop spreads over a dry porous layer. The problem is treated under the lubrication theory approximation and in the case of complete wetting. Spreading of "big drops" (but still small enough to neglect the gravity action) over "thin porous layers" is considered below.

The kinetics of liquid motion both in the drop above the porous layer and inside the porous layer itself are taken into account below. The thickness of the porous layer $\Delta$, is assumed to be much smaller than the drop height, that is, $\Delta \ll h^*$ ,where $h^*$ is the scale of the drop height. The drop profile is assumed having a low slope ($h^*/L^* \ll 1$, where $L^*$ is the scale of the drop base), and the influence of the gravity is neglected (small drops, Bond number $\rho g L^{*2}/\gamma \ll 1$, where $\rho$, $g$, and $\gamma$ are the liquid density, gravity acceleration, and the liquid–air interfacial tension, respectively). That is, only capillary forces are taken into account.

Under such assumptions, a system of two differential equations has been deduced [1,2] to describe the evolution with time of the radius of both the drop base, $L(t)$, and the wetted region inside the porous layer, $l(t)$ (Fig. 1):

$$\frac{dL}{dt} = 0.1\left(\frac{4(V_0 - \pi m \Delta l^2)}{\pi}\right)^{0.3}\left(\frac{10\gamma\omega}{\mu}\right)^{0.1}\frac{1}{(t+t_0)^{0.9}} - \frac{2\pi m \Delta K_p p_c L/\mu}{3(V_0 - \pi m \Delta l^2)\ln\frac{l}{L}}, \quad (1)$$

$$\frac{dl}{dt} = \frac{K_p p_c/\mu}{l\ln\frac{l}{L}}, \quad (2)$$

where $t$ is time, $V_0$, $\gamma$, and $\mu$ are an initial drop volume, interfacial tension, and dynamic viscosity, respectively, $m$, $\Delta$, $K_p$, and $p_c$ are the porosity, the thickness, permeability, and effective capillary pressure of the porous layer, respectively, $\omega \cong 0.01$ is an effective lubrication coefficient [3], and $t_0$ is the duration of the initial stage [3], when the capillary regime of spreading is not applicable.

Let $t^*$ be the time instant when the drop is completely sucked by the porous substrate $V(t^*)=0=V_0-\pi m \Delta l^{*2}$, where $l^*$ is the maximum radius of the wetted region in the porous layer. The latter equation gives:

$$l^* = \left(\frac{V_0}{\pi m \Delta}\right)^{1/2} \quad (3)$$

$l^*$ is used below to scale the radius of the wetted region in the porous layer, $l(t)$. It is easy to check that the latter equation results in $l^* > L^*$ in the case under consideration.

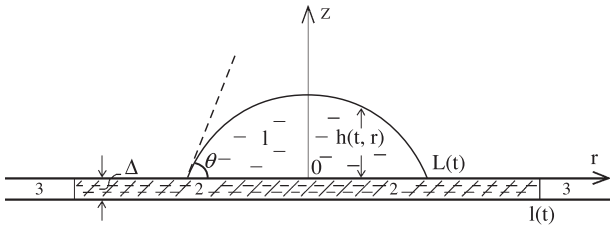


Fig. 1. Cross section of the axisymmetric spreading drop over initially dry thin porous substrate with thickness Δ. 1, Liquid drop; 2, wetted region inside the porous substrate; 3, dry region inside the porous substrate; $L(t)$ radius of the drop base; $l(t)$ radius of the wetted area inside the porous substrate; Δ thickness of porous substrate; $r$, $z$ coordinate system; $h(t, r)$ profile of the spreading drop.

An estimation of the time scale $t^*$ can be made as [1,2]:

$$t^* = \frac{V_0 \ln\frac{l^*}{L^*}}{\pi m \Delta K_p p_c/\mu} \quad (4)$$

It has been shown [1,2] that the dynamic contact angle asymptotically remains constant in the second stage. This constant value is marked below as $\theta_e$. Let us introduce $\theta_m = \frac{\pi V_0}{4L_m^3}\left(1 - l_m^2/l^{*2}\right)$, which is the value of the dynamic contact angle at the time instant when the maximum value of the drop base is reached. Then $\theta/\theta_m$ should be a universal function of the dimensionless time, $t/t^*$. This conclusion agrees well with experimental observations [1,2]. It is necessary to emphasize that in the case under consideration, the constancy of the contact angle has nothing to do with the contact angle hysteresis: there is no hysteresis in the system under consideration. $\theta_e$ is not a receding contact angle but forms as a result of a self-regulation of the flow in the drop-porous layer system.

System of Eqs. (1) and (2) includes seven parameters, five of which can be measured directly ($V_0$, $\gamma$, $\mu$, $m$, and $\Delta$ are the initial volume of the drop, the liquid–air interfacial tension, the liquid viscosity, the porosity of the porous layer, and the thickness, respectively) and two additional parameters, $\omega$ and $K_p p_c$, which should be determined independently. Noteworthy that the porous layer permeability and the capillary pressure always enter as a product, that is, this product can be considered as a single parameter. A procedure of independent determination of an effective lubrication coefficient, $\omega$, has been discussed in Ref. [3].

Silicone oils SO20 (viscosity 0.218 P), SO50 (viscosity 0.554 P), SO100 (viscosity 1.18 P), and SO500 (viscosity 5.582 P) purchased from 'PROLABO' were used in the spreading experiments [1,2]. Cellulose nitrate membrane filters, purchased from Sartorius (type 113), with pore size $a$=0.2 and $a$=3 μm (marked by the supplier) were used as porous layers. These membranes are referred below as the membrane $a$=0.2 μm and the membrane $a$=3 μm, respectively.

As mentioned above, the permeability of the porous layer and the capillary pressure always enter as a product, i.e., as a

single coefficient. Additional experiments were carried out to determine this coefficient. For this purpose, the horizontal imbibition of the liquid under investigation into the dry porous sheet was undertaken. Rectangular sheets 1.5×3 cm were used. Those porous sheets were cut from the same membranes used in the spreading experiments. Each sheet was immersed on 0.3–0.5 cm into a liquid container, and the position of the imbibition front was monitored over time. In the case under investigation, a unidirectional flow of liquid inside the porous substrate took place. Using Darcy's law, we can conclude that $d^2(t)=2K_p p_c t/\mu$, where $d(t)$ is the position of the imbibition front inside the porous layer. It was found that in all runs, $d^2(t)/2$ proceeds along a straight line, whose slope gives us $K_p p_c$ value. $K_p p_c$ values were found independent of the tested liquid viscosity [1,2] in accordance with the theory predictions [4].

Table 1 shows that the final value of the dynamic contact angle, $\theta_e$ (last column in Table 1), depends on the volume of the drop, as well as on the viscosity of the liquid, and hence, $\theta_e$ is determined solely by hydrodynamics.

Fig. 2a presents experimentally measured dependencies of radius of the drop base and the wetted region inside the porous layer on time for different silicone oils, porous layers, and drop volumes. All relevant values are summarized in Table 1. The main result appears in Fig. 2b, which shows that all experimental data (the same as in Fig. 2a) fall on two universal curves if dimensionless coordinates are selected as follows: $\bar{L}=L/L_m$, $\bar{l}=l/l^*$, and $\bar{t}=t/t^*$, where $L_m$ is the maximum value of the drop base, which is reached at the time instant $t_m$. The same symbols (with an over bar) are used for dimensionless values as for dimensional. The scale $l^*$ is determined by Eq. (3) and the time scale $t^*$ is given by Eq. (4). In Fig. 2b, the solid lines are calculated according to Eqs. (1) and (2).

The 12th column in Table 1 gives the experimental values of the dynamic contact angle, $\theta_m$, which the drop has when the drop base reaches its maximum value, $L_m$. These values were used for plotting the time evolution of the dynamic contact angle, $\theta/\theta_m$. Fig. 3 shows that all experimental points fall on a single universal curve, as predicted by Eqs. (1) and (2).

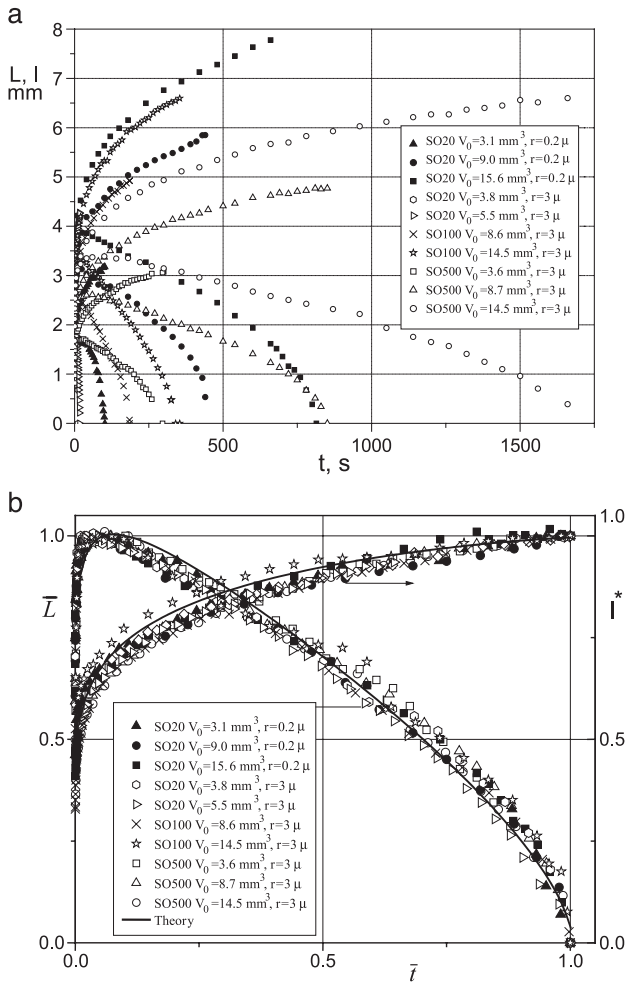


Fig. 2. (a) Measured dependencies of radii of the drop base ($L$, mm) and radii of the wetted region inside the porous layer ($l$, mm) on time ($t$, s). All relevant values are summarized in Table 1. (b) The same as in (a) but using dimensionless coordinates: $\bar{L}=L/L_m$, $\bar{l}=l/l^*$, $\bar{t}=t/t_p^*$, where $L_m$ is the maximum value of the drop base, which is reached at the moment $t_m$. The same symbols (with overbar) are used for dimensionless values as for dimensional ones. $l^*$ and $t_p^*$ according to Eqs. (3) and (4), respectively. Solid lines according to Eqs. (1) and (2).

The solid line in Fig. 3 is a result of calculations according to Eqs. (1) and (2), where dimensionless dependencies $\bar{L}(\bar{l})$ and $\bar{l}(\bar{t})$ are taken from previous Fig. 2b.

Table 1
Relevant values for measurement of dependencies of radii of the drop base ($L$, *mm*) and radii of the wetted region inside the porous layer ($l$, *mm*) on time ($t$, *s*) in Figs. 2a and b

| Liquid | Notation in figures | Membrane pore size (μm) | $V_0$ (ml×10$^3$) | Δ (mm) | $m$—Porosity | $t_p^*$ (s) | $l^*$ (cm) | $l^*$ (theory) | $L_m$ (cm) | $L_m$ (theory) | $\theta_m$ (°) | $\theta_e$ (°) |
|---|---|---|---|---|---|---|---|---|---|---|---|---|
| SO20 | ▲ | 0.2 | 3.1 | 0.114 | 0.85 | 102 | 0.318 | 0.317 | 0.179 | 0.184 | 20.0 | 12 |
| SO20 | ● | 0.2 | 9.0 | 0.116 | 0.72 | 440 | 0.585 | 0.584 | 0.314 | 0.31 | 12.6 | 11.4 |
| SO20 | ■ | 0.2 | 15.6 | 0.116 | 0.73 | 814 | 0.77 | 0.766 | 0.387 | 0.39 | 14.2 | 12.1 |
| SO20 | ○ | 3 | 3.8 | 0.136 | 0.87 | 10.9 | 0.345 | 0.319 | 0.196 | 0.198 | 25.9 | 22.3 |
| SO20 | ▷ | 3 | 5.5 | 0.134 | 0.83 | 17.1 | 0.428 | 0.398 | 0.223 | 0.234 | 20.3 | 18.6 |
| SO100 | × | 3 | 8.6 | 0.137 | 0.82 | 186 | 0.493 | 0.494 | 0.257 | 0.274 | 18.5 | 11 |
| SO100 | ☆ | 3 | 14.5 | 0.138 | 0.77 | 354 | 0.659 | 0.659 | 0.332 | 0.34 | 15.5 | 17.2 |
| SO500 | □ | 3 | 3.6 | 0.138 | 0.89 | 296 | 0.306 | 0.306 | 0.174 | 0.179 | 22.6 | 19.4 |
| SO500 | △ | 3 | 8.7 | 0.138 | 0.88 | 851 | 0.477 | 0.478 | 0.264 | 0.286 | 19.1 | 17.3 |
| SO500 | ○ | 3 | 14.5 | 0.136 | 0.78 | 1660 | 0.66 | 0.660 | 0.339 | 0.34 | 15.8 | 16.5 |

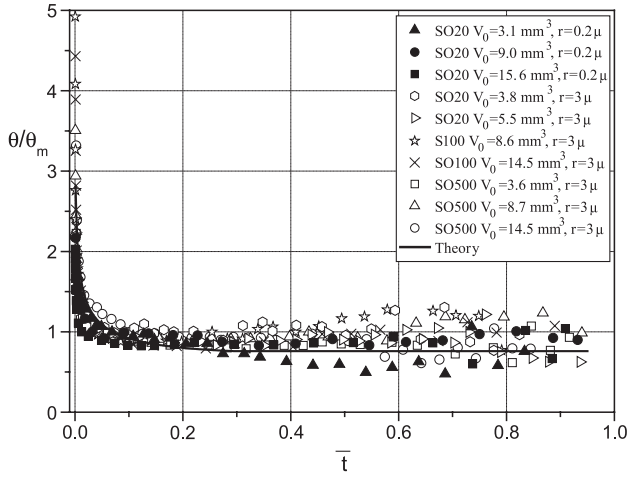


Fig. 3. Dynamic contact angle on the dimensionless time. Solid line according to Eqs. (1) and (2).

Below, the similar dimensionless scales are used in the case of spreading of surfactant solutions over porous substrates.

## 2. Spreading of surfactant solutions over dry porous substrates, hysteresis phenomena

In this section, we take up the same problem in the case when a drop spreads over a dry porous layer in the case of partial wetting. Spreading of "big drops" (but still small enough to neglect the gravity action) of aqueous SDS solutions over "thin porous layers" (nitrocellulose membrane) is considered below according to Ref. [5].

Aqueous solutions of sodium dodecyl sulfate (SDS) (an anionic surfactant) were used in the spreading experiments. The following SDS concentrations were used: zero concentration (pure water), concentrations below CMC, near CMC, and above CMC [5]. SDS was purchased from Fisher Scientific and used as obtained, without purification. Nitrocellulose membranes, purchased from Millipore, with averaged pore size $a$=0.22, $a$=0.45 and $a$=3.0 μm (marked by the supplier) were used as a model of thin porous layers.

The same experimental chamber as in Section 1was used for monitoring of the spreading of liquid drops over initially dry porous substrates. The time evolution of the radius of the drop base, $L(t)$, the dynamic contact angle, $\theta(t)$, and the radius of the wetted area inside the porous substrate, $l(t)$, were monitored (Fig. 1).

A modified experimental setup (as compared with the previous case) was used for measurements of static advancing and receding contact angles on a nonporous nitrocellulose substrate [5].

In all spreading experiments [5], the drops remained the spherical shape over the whole spreading process. This was cross-checked by reconstruction of the drop profiles at different time instants of spreading, fitting those drop profiles by a spherical cap.

According to observations, the whole spreading process can be subdivided into three stages (see Fig. 4) [5]. During the *first stage*, the contact angle, $\theta$, rapidly decreases while the radius of the drop base, $L$, increases until its maximum value, $L_m$. The first stage was followed by the *second stage*, when the radius of the drop base, $L$=$L_m$, was constant, and the contact angle, $\theta$, decreased linearly with time. During the *third stage*, the radius of the drop base decreased and the contact angles remained constant. At the final third stage, the drop base shrank until the drop completely disappeared and the imbibition front expanded until the end of the process. The spherical form of the spreading drop allows measuring the evolution of the contact angle of the spreading drops. The contact angle, $\theta$, during the first stage decreased very fast, during the second stage, the contact angle, $\theta$, decreased much slower and linearly, and the contact angle remained a constant value over the duration of the third stage. This constant value of the contact angle is referred below as $\theta_e$.

All relevant experimental data are summarized in Table 2.

It is possible to show that that the dependency of the contact angle during the second stage of the spreading is a linear function of time [5].

Everywhere below, the time evolution is presented of both the radius of the base of the spreading drops and the radius of the wetted area using dimensionless coordinates. The drops were of different volumes and different SDS

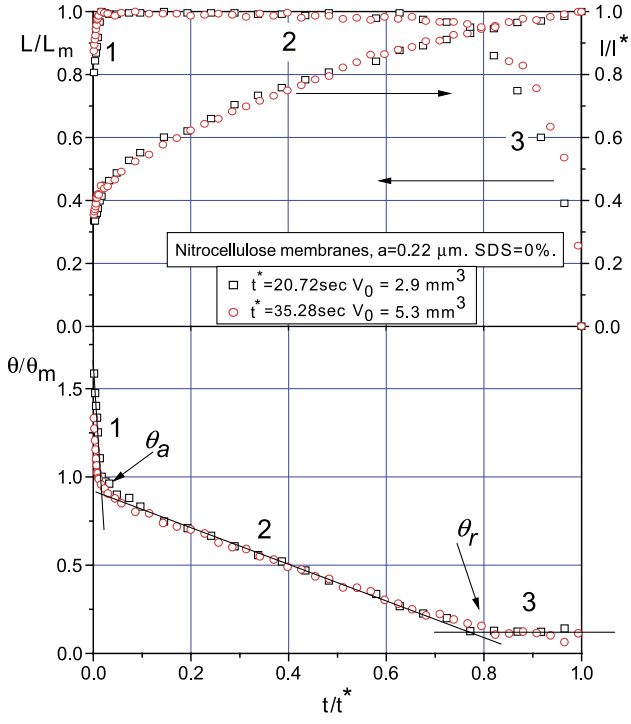


Fig. 4. Spreading of pure aqueous drops over nitrocellulose membrane $a$=0.22 μm. $L/L_m$, dimensionless radius of the drop base, $l/l^*$, radius of the wetted area, $\theta/\theta_m$, dynamic contact angle, $t/t^*$, dimensionless time. 1—first stage: $\theta$ rapidly decreases while $L$ increases until the maximum value $L_m$. 2—second stage: $L$ is constant, $L$=$L_m$, and $\theta$ decreases linearly with time. 3—third stage: $L$ decreases and $\theta$ remains constant.

Table 2
Relevant values for measurement of dependencies of radii of the drop base ($L$, *mm*) and radii of the wetted region inside the porous layer ($l$, *mm*) on time ($t$, *s*) in Figs. 4–8

| Pore size, figure symbols | Averaged pore size (μm) | SDS concentration (%) | $V_0$, initial volume of the drop (μl) | $t^*$ (s) | $L_m$ (mm) | $l^*$ (mm) | $\theta_m$ (grad) | $t_m$ (s) |
|---|---|---|---|---|---|---|---|---|
| Fig. 4 squares | 0.22 | 0 | 2.9 | 20.72 | 1.49 | 3.38 | 51 | 0.36 |
| Fig. 4 circles | 0.22 | 0 | 5.3 | 35.28 | 1.85 | 4.13 | 50 | 0.36 |
| Fig. 5 squares | 3.0 | 0.1 | 2.1 | 2.96 | 1.47 | 2.30 | 31 | 0.36 |
| Fig. 5 triangles | 3.0 | 0.1 | 3.7 | 4.92 | 2.01 | 3.40 | 24 | 0.64 |
| Fig. 5 circles | 3.0 | 0.1 | 9.7 | 13.12 | 2.59 | 5.28 | 35 | 0.48 |
| Fig. 6 diamonds | 0.22 | 0 | 2.9 | 20.72 | 1.49 | 3.38 | 51 | 0.36 |
| Fig. 6 circles | 0.22 | 0.1 | 10.5 | 75.2 | 2.78 | 5.79 | 32 | 0.4 |
| Fig. 6 squares | 0.22 | 0.2 | 7.4 | 33.84 | 2.45 | 4.67 | 27 | 0.44 |
| Fig. 6 triangles | 0.22 | 0.5 | 2.6 | 8.2 | 2.03 | 2.90 | 20 | 0.12 |
| Fig. 7 diamonds | 0.45 | 0 | 6.1 | 8.44 | 2.83 | 4.35 | 44 | 0.52 |
| Fig. 7 circles | 0.45 | 0.1 | 9.5 | 10.28 | 2.46 | 4.92 | 38 | 0.35 |
| Fig. 7 squares | 0.45 | 0.2 | 7.2 | 8.44 | 2.83 | 4.35 | 21 | 0.36 |
| Fig. 7 triangles | 0.45 | 0.5 | 7.1 | 6.84 | 2.75 | 4.80 | 23 | 0.08 |
| Fig. 8 diamonds | 3.0 | 0 | 5.9 | 108.04 | 1.89 | 4.21 | 46 | 21 |
| Fig. 8 circles | 3.0 | 0.1 | 9.7 | 13.12 | 2.59 | 5.28 | 35 | 0.48 |
| Fig. 8 squares | 3.0 | 0.2 | 6.8 | 3.96 | 2.65 | 4.43 | 21 | 0.28 |
| Fig. 8 circles | 3.0 | 0.5 | 5.1 | 2.12 | 2.39 | 3.97 | 22 | 0.12 |

concentrations. The total duration of the spreading process, $t^*$, the maximum radius of the drop base, $L_m$, and the final radius of the wetted area, $l^*$, vary considerably depending on the drop volume, SDS concentration, the averaged pore size, and porosity of nitrocellulose membranes. It has been suggested in the first section to use the following dimensionless values: $L/L_m$, $l/l^*$, and $t/t^*$. The same dimensionless values are used below. According to the first section, the reduced contact angle dependency, $\theta/\theta_m$, against dimensionless time $t/t^*$ is used below, where $\theta_m$ is the value of the dynamic contact angle, which is reached at the moment $t=t_m$ (the end of the first stage of the spreading process).

Fig. 4 shows that spreading behaviour of drops of different volumes over the same porous substrate has a universal character in dimensionless coordinates. However, not all of the experimental data have shown such universal behaviour. Some experimental runs differ during the first stage of spreading in dimensionless coordinates (Fig. 5). This difference becomes bigger if overall time of spreading is shorter (droplets of different volumes).

In Figs. 6–8 (0.22, 0.45, and 3.0 μm nitrocellulose membranes, respectively), the time evolution is presented of the radius of the drop base, the radius of the wetted area inside the porous substrates, and the contact angle at different SDS concentrations.

Figs. 6–8 show that the second stage of spreading becomes shorter in dimensionless coordinates with the increase in SDS concentration. Contact angles show the universal constant behaviour during the third stage of spreading for each of SDS concentrations.

### *2.1. Advancing and hydrodynamic receding contact angles on porous nitrocellulose membranes*

Using presented experimental data on spreading of drop of aqueous SDS solutions over dry porous substrates, the values of advancing, $\theta_a$, and hydrodynamic receding, $\theta_{rh}$, contact angles were extracted as function of SDS concentration. We are using below the term "hydrodynamic receding contact angle" and the symbol $\theta_{rh}$ to distinguish it from the static receding contact angle, which is found

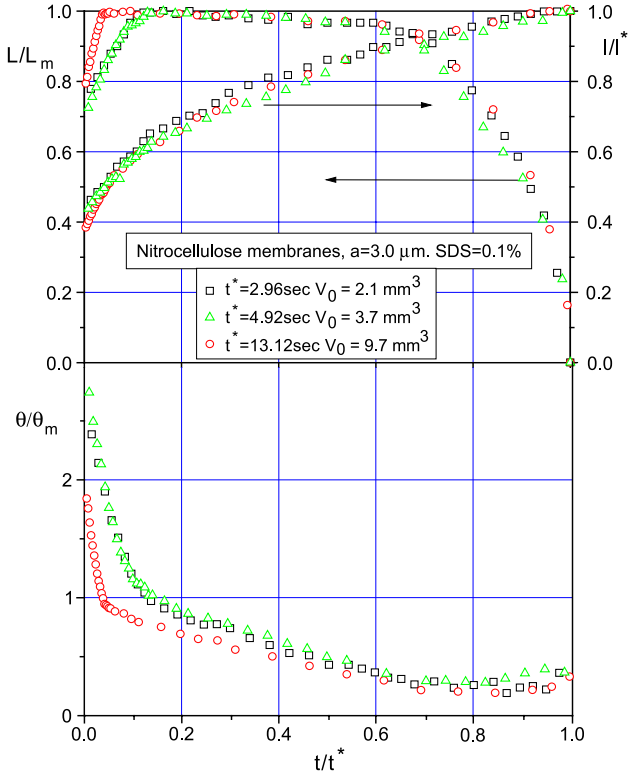


Fig. 5. Spreading of droplets of 0.1% SDS solution over nitrocellulose membrane, $a$=3.0 μm. $L/L_m$ dimensionless radius of the drop base, $l/l^*$ radius of the wetted area, $\theta/\theta_m$, dynamic contact angle, $t/t^*$ dimensionless time.

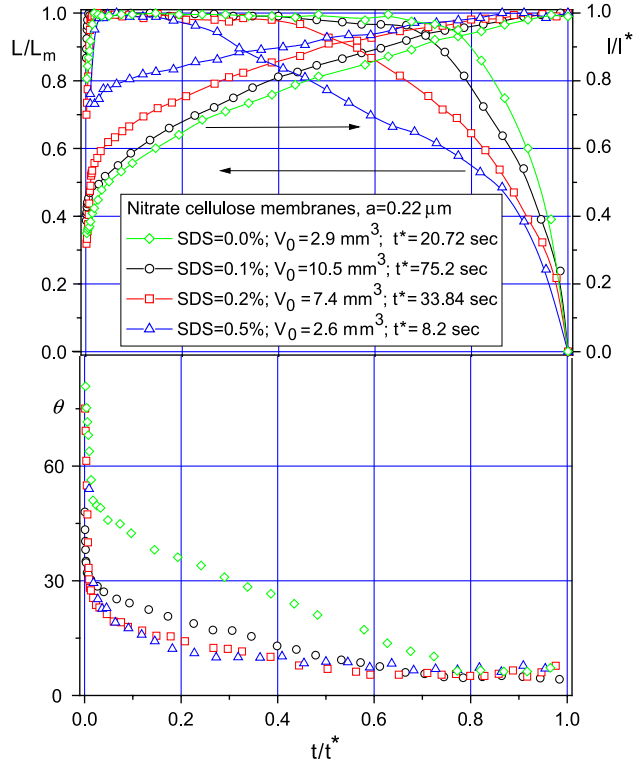


Fig. 6. Spreading of droplets of SDS solutions over nitrocellulose membrane, $a$=0.22 μm. $L/L_m$, dimensionless radius of the drop base, $l/l^*$, radius of the wetted area, $\theta/\theta_m$, dynamic contact angle, $t/t^*$, dimensionless time.

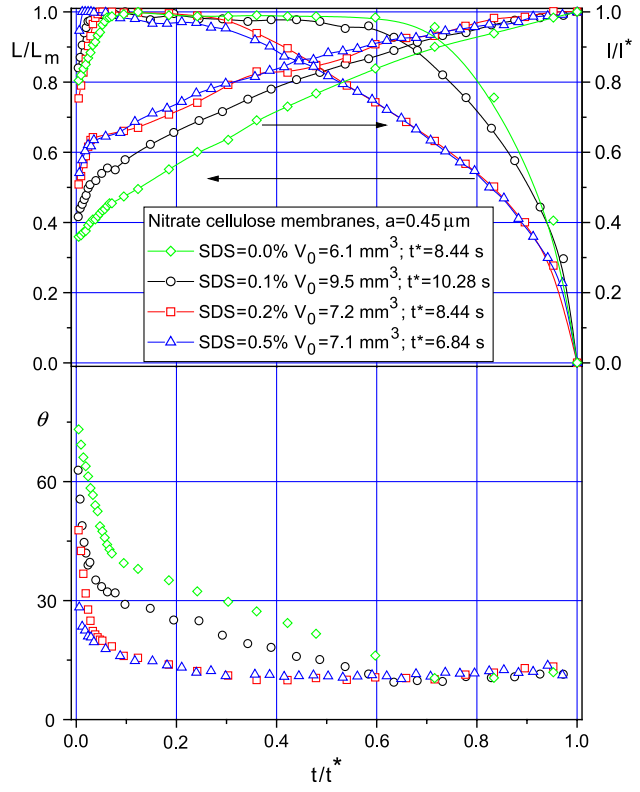


Fig. 7. Spreading of droplets of SDS solutions over nitrocellulose membrane, $a$=0.45 μm. $L/L_m$, dimensionless radius of the drop base, $l/l^*$, radius of the wetted area, $\theta/\theta_m$, dynamic contact angle, $t/t^*$, dimensionless time.

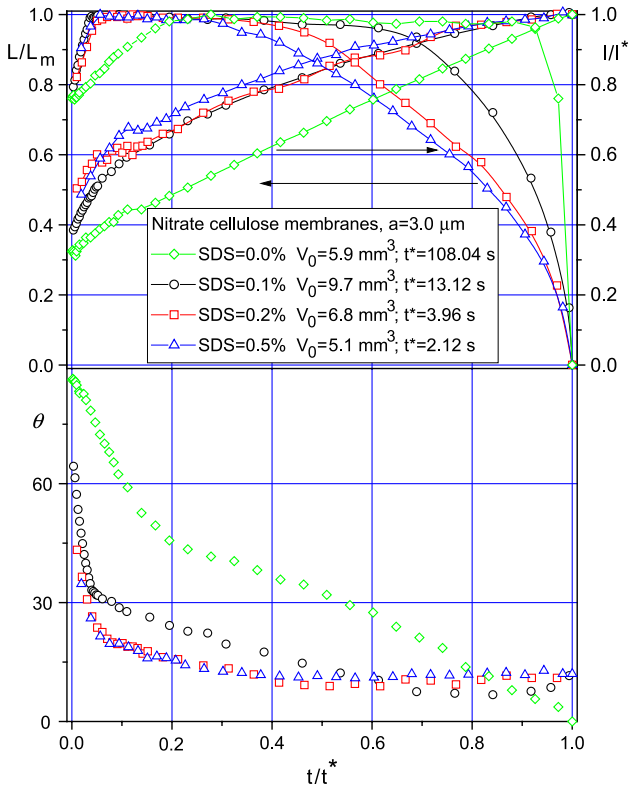


Fig. 8. Spreading of droplets of SDS solutions over nitrocellulose membrane, $a$=3.0 μm. $L/L_m$, dimensionless radius of the drop base, $l/l^*$, radius of the wetted area, $\theta/\theta_m$, dynamic contact angle, $t/t^*$, dimensionless time.

equal to zero (see Section 2.2). The advancing contact angle, $\theta_a$, was defined at the end of the first stage when the drop stopped to spread (the radius of the drop base reached its maximum value). The hydrodynamic receding contact angle, $\theta_{rh}$, was defined at the moment when the drop base started to shrink.

In Fig. 9, experimental data on the apparent contact angle hysteresis are summarized. This figure shows that the advancing contact angle, $\theta_a$, decreases with SDS concentration; the hydrodynamic receding contact angle, $\theta_{rh}$, on the contrary, slightly increases with SDS concentration.

These experimental runs show that: the difference between advancing and receding contact angles becomes smaller with the increase in the SDS concentration (Fig. 9); the dimensionless time interval when the drop base does not move also decreases with the increase in the SDS concentration.

### *2.2. Static hysteresis of the contact angle of SDS solution drops on smooth nonporous nitrocellulose substrate*

Above, the spreading of drops at different SDS concentrations on nitrocellulose membranes of various pore sizes was considered. In all cases, during the third stage of spreading, the radius of the drop base, $L$, shrank and the hydrodynamic receding contact angle, $\theta_{rh}$,

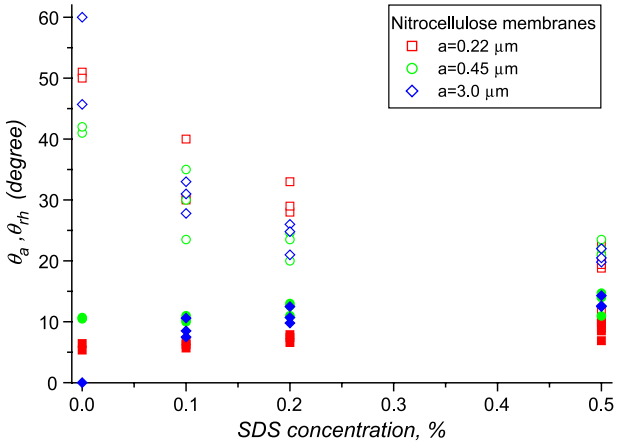


Fig. 9. Porous nitrocellulose substrates. Apparent contact angle hysteresis variation with SDS concentration. Nitrocellulose membranes of different average pore sizes. Open symbols correspond to the advancing contact angle, $\theta_a$. The same filled symbols correspond to the hydrodynamic receding contact angle, $\theta_{rh}$.

remained constant. The duration of the third stage of spreading increases with the SDS concentration increase. It is necessary to note that the behaviour of drops of aqueous SDS solutions during the third stage of spreading (partial wetting) is remarkably similar to the behaviour during the second stage of spreading in the case of complete wetting (see Section 1).

It was found above that the advancing and hydrodynamic receding contact angles are strongly dependent on the SDS concentration on porous nitrocellulose membranes.

It has been decided to carry out measurements of static advancing and static receding contact angles on smooth nonporous nitrocellulose substrate for different SDS concentrations [5]. The idea is to compare hysteresis of contact angles on the smooth nonporous nitrocellulose substrate with the hysteresis contact angles obtained earlier on porous nitrocellulose substrates at corresponding SDS concentrations.

Static advancing contact angle values were obtained using direct spreading experiments. A droplet of SDS solution was deposited from above on the smooth nonporous nitrocellulose substrate. Dynamics of the droplet spreading was monitored. The final value of the contact angle under this experimental condition was equal to the static value of the advancing contact angle.

The static advancing contact angle of pure water on nonporous nitrocellulose substrate was found equal approximately to 70°. The static advancing contact angle decreases with the increase of SDS concentration (Fig. 10). This trend continues until the CMC is reached. At concentrations above the CMC, advancing contact angle remains constant and approximately equals 35°.

The receding contact angle values were obtained using completely different experimental procedure. In this case, the contact angle dynamics was investigated using linearly decreasing droplet volume [5].

Nonzero value of the static receding contact angle was found only in the case of pure water droplets. In all other cases (even at the smallest SDS concentrations used 0.025%), the static receding contact angle was found equal to zero in the whole concentration range used: from 0.025% (10 times smaller than CMC) to 1% (5 times higher than CMC).

Both static receding and static advancing contact angles on smooth nonporous nitrocellulose substrate against SDS concentration are presented in Fig. 10.

The results highlight a linear decline of the static advancing contact angle from 70° at 0% SDS (pure water) to approximately 35° at the value of the CMC (2.4%); after that, the static advancing contact angle reaches a steady value which remains constant irrespective of further increase in the SDS concentration. In contrast to that, the static receding contact angle is approximately equal to 45° for the pure water and is equal to zero in the presence of SDS even at concentrations as low as 0.025%.

Comparison of Fig. 9 and Fig. 10 shows:

- The advancing contact angle dependence on SDS concentration on porous nitrocellulose substrates is significantly different from the static advancing contact angle dependence on nonporous nitrocellulose substrates. The latter means that in the case of porous substrates, influence of both the hydrodynamic flow caused by the imbibition into the porous substrate and the substrate roughness changes significantly the advancing contact angle.
- The hydrodynamic receding contact angle in the case of the porous substrates has nothing to do with the hysteresis of the contact angle and determined complete by the hydrodynamic interactions in the way similar to the complete wetting case (see Section 1).

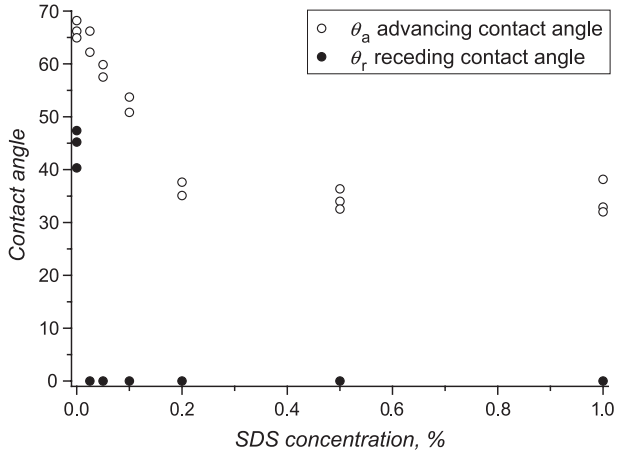


Fig. 10. Advancing and receding contact angles variation with SDS concentration on nonporous nitrocellulose substrate. Open symbols correspond to the static advancing contact angle, $\theta_a$. Filled symbols correspond to the static receding contact angle, $\theta_r$.

## 3. Spontaneous imbibition and capillary rise of surfactant solutions into hydrophobic capillaries

Pure water does not penetrate spontaneously into hydrophobized quartz capillaries; however, surfactant solutions penetrate spontaneously and the penetration rate depends on the concentration of surfactant. Both the air–liquid interfacial tension, $\gamma$, and the contact angle of the moving meniscus, $\theta_a$, are concentration-dependent [6], where a subscript a indicates the advancing contact angle.

As shown in Ref. [6], the adsorption of surfactant molecules behind the moving meniscus results in a decrease of the bulk surfactant concentration starting from the capillary inlet in the direction of the moving meniscus. However, the major process, which determines the penetration of surfactant solutions into hydrophobic capillaries or spreading of surfactant solutions over hydrophobic substrates, is the adsorption of surfactant molecules onto a bare hydrophobic substrate in front of the moving three-phase contact line [6,7]. The latter process results in a partial hydrophilisation of the hydrophobic surface in front of the meniscus/drop, which, in its turn, determines the spontaneous imbibition/spreading.

Let us consider a very beginning of the imbibition process when a meniscus of a surfactant solution touched for the first time an inlet of the hydrophobic capillary. The contact angle, $\theta_a$, at this moment is bigger than $\pi/2$ and the liquid cannot penetrate into the hydrophobic capillary. The solid–liquid and liquid–air interfacial tensions, $\gamma_{SL}$ and $\gamma$, respectively, are assumed to not vary with time because the adsorption of surfactant molecules onto these surfaces is a fast process as compared with the rate of the imbibition. The only interfacial tension, which can vary, is the solid–air interfacial tension, $\gamma_{SV}$. If the adsorption on the solid–air interface does not occur, then the spontaneous imbibition into a hydrophobic capillary cannot take place spontaneously because the advancing contact angle remains above $\pi/2$. However, if the adsorption of surfactant molecules on the bare hydrophobic surface in a vicinity of the three-phase contact line takes place, then $\gamma_{SV}$ grows with time. After some critical surface adsorption, $\Gamma_{SVcr}$, is reached, then the advancing contact angle reaches $\pi/2$. Only after that the spontaneous imbibition process starts. The latter consideration shows that there is a critical bulk concentration, $C^*$, below which $\Gamma_{SV}$ remains below its critical value, $\Gamma_{SVcr}$, and the spontaneous imbibition process does not take place.

In the case of partial wetting, the capillary imbibition in the horizontal direction proceeds according to the following dependency:

$$\ell = \sqrt{\frac{r\gamma\cos\theta_a}{2\mu}t} \tag{5}$$

where $l$ is the length of the part of the capillary filled with the liquid, $r$ is the radius of the capillary, $\mu$ is the liquid viscosity, $\theta_a$ is the advancing contact angle, which is above $\pi/2$: $0<\theta_a<\pi/2$, and $t$ is time.

A pure water does not penetrate into hydrophobic capillaries and shows the advancing contact angle, $\theta_a>\pi/2$. The latter means that the liquid can be only forced into the capillary and does not penetrate spontaneously. However, the advancing contact angle is a decreasing function of the surfactant concentration, and at some critical concentration, $C^*$, $\theta_a$ becomes equal to $\pi/2$. The latter means that above $C^*$, surfactant solution penetrates spontaneously into hydrophobic capillaries.

Both the surfactant molecules transfer and the liquid viscosity control the penetration in the case of the imbibition of surfactant solutions into hydrophobic capillaries according to Eq. (5). In this case, the aim is to reveal the mechanism of the penetration and to determine the concentration of surfactant molecules near the meniscus $C_m<C_0$, where $C_0$ is the surfactant concentration at the capillary inlet. Fig. 11 shows that in the case of Syntamid-5, the advancing contact angle, $\theta_a$, exceeds 90° at concentration $C^*$, which is slightly under 0.05% [6].

Below, we show that both the bulk diffusion and the surface diffusion of surfactant molecules (including that on the unwetted portion of the capillary in front of the moving meniscus) play an important role and a theory is presented for this case.

### 3.1. Theory

Let us consider a dependency of $\Psi(C_m)=\gamma(C_m)\cos\theta_a(C_m)$ on the concentration of surfactant, $C_m$, on the moving meniscus. According to the triangle rule, it can be calculated as:

$$\Psi(C_m) = \gamma_{SV}(C_m) - \gamma_{SL}(C_m) \tag{6}$$

where $\gamma_{SV}$ and $\gamma_{SL}$ are solid–vapor and solid–liquid interfacial tensions, respectively. According to Antonov's

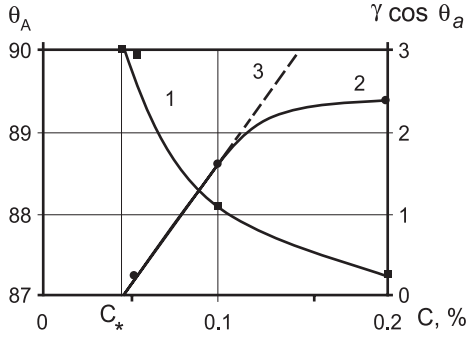


Fig. 11. The influence of concentration of aqueous surfactant solutions (Syntamide-5, molecular weight 420) on the advancing contact angle $\theta_a$ (curve 1) and $\gamma\cos\theta_a$ (curve 2) measured on a flat hydrophobized quartz surface. $C^*$ marks the critical surfactant concentration, below which surfactant solution does not spread. Broken line 3 according to Eq. (10).

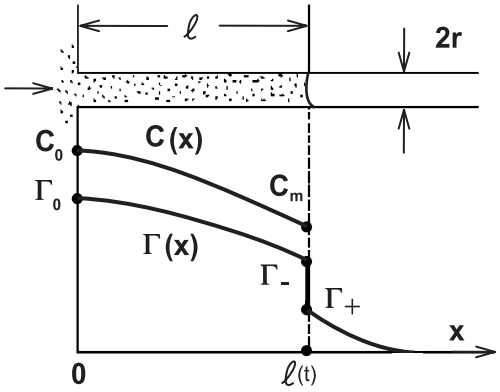


Fig. 12. Bulk volume, $C$, and surface, $\Gamma$, distribution of surfactant concentrations along the capillary length during a spontaneous imbibition process.

rule, the dependency of two latter interfacial tensions on the concentration can be presented as

$$\gamma_{SV}(C_m) = \gamma^0_{SV}\left(1 - \frac{\Gamma_+}{\Gamma^\infty}\right) + \gamma^\infty_{SV}\frac{\Gamma_+}{\Gamma^\infty};$$
$$\gamma_{SL}(C_m) = \gamma^0_{SL}\left(1 - \frac{\Gamma_-}{\Gamma^\infty}\right) + \gamma^\infty_{SL}\frac{\Gamma_-}{\Gamma^\infty}, \quad (7)$$

where superscripts 0 and $\infty$ mark zero and complete coverage of hydrophobic adsorption sites, respectively, subscripts + and − mark adsorption just behind and just in front of the moving meniscus, respectively, and $\Gamma$ is the surface adsorption of surfactant molecules.

Note that adsorption of surfactant molecules results in a decreasing of SL interfacial tension, that is, $\gamma^0_{SL}-\gamma^\infty_{SL}>0$. However, adsorption of surfactant molecules on the bare hydrophobic interface in front of the moving meniscus results in a local increase of the SV interfacial tension, that is, $\gamma^0_{SV}-\gamma^\infty_{SV}<0$. The initial contact angle on the bare hydrophobic interface is assumed bigger than $\pi/2$, that is, $\gamma^0_{SV}-\gamma^0_{SL}<0$.

It is assumed below that both adsorption isotherms are linear functions of the surfactant concentration below CMC and remain constant above CMC. The latter means

$$\Gamma_- = G_{SL}C_m \quad (8)$$

at concentrations below CMC.

Both a spontaneous imbibition and a spontaneous capillary rise into hydrophobic capillaries are sufficiently slow processes, that is, we assume below a condition of local equilibrium on the moving three-phase contact line. According to this assumption, the equality of chemical potentials of adsorbed surfactant molecules should be satisfied across the three-phase contact line, that is, ln $\Gamma_-+\Phi_{SL}$=ln $\Gamma_+ + \Phi_{SV}$, where $\Gamma_-$ and $\Gamma_+$ are jumps of adsorption across the meniscus surface (Fig. 12), and $\Phi_{SL}$ and $\Phi_{SV}$ (in kT units) are the corresponding values of the energy of surfactant molecules at solid–water and solid–air interfaces, respectively. From the latter equation, we conclude: $\Gamma_+ = \frac{\Gamma_-}{\exp(\Phi_{SV}-\Phi_{SL})}$. It is obvious that $\Phi_{SV}$ is higher than $\Phi_{SL}$, and hence, $\Gamma_+<\Gamma_-$. The latter relation can be rewritten using Eq. (8) as

$$\Gamma_+ = G_{SV}C_m, G_{SV} = \frac{G_{SL}}{\exp(\Phi_{SV} - \Phi_{SL})} \quad (9)$$

Substitution of Eqs. (7) Eqs. (8) Eqs. (7) into Eq. (6) and having in mind the latter inequalities, we can conclude after rearrangements that

$$\Psi(C_m) = \alpha(C_m - C_*) \quad (10)$$

where

$$\alpha = \left[\frac{G_{SV}}{\Gamma^\infty}\left(\gamma^\infty_{SV} - \gamma^0_{SV}\right) + \frac{G_{SL}}{\Gamma^\infty}\left(\gamma^0_{SL} - \gamma^\infty_{SL}\right)\right] > 0, \quad C_* = \frac{\alpha^0}{\alpha},$$
$$\alpha^0 = \gamma^0_{SL} - \gamma^0_{SV} > 0$$

According to Eq. (10), $\Psi(C_m)$ dependency should be a linear function of concentration at $C_m>C_*$, which is the good agreement with experimental observations (line 3 in Fig. 11 at concentrations to $C_*$).

We now try to solve theoretically the problem of a spontaneous imbibition of surfactant solutions into hydrophobic cylindrical capillaries taking into account the convective transfer and the surface diffusion of surfactant molecules as well as adsorption on a bare hydrophobic surface in front of the moving meniscus. The location of the moving meniscus in the capillary is $l(t)$ (Fig. 12).

A characteristic time scale of the equilibration of the surfactant concentration in a cross section of the capillary,

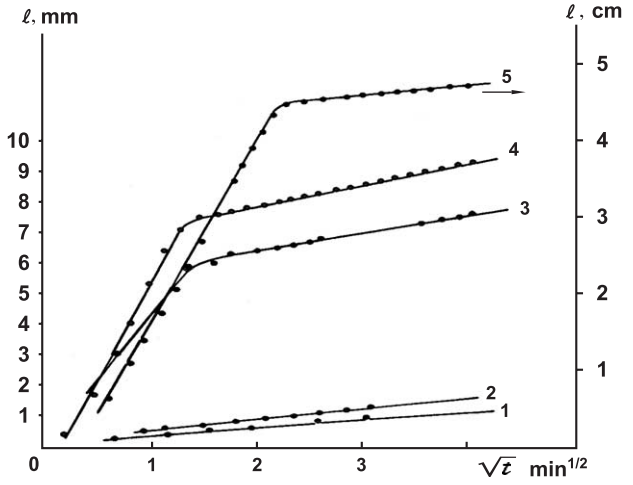


Fig. 13. The time evolution of the imbibition length $l$ (mm) with time $t$ (min) for aqueous solutions of Syntamide-5 in a horizontal hydrophobized quartz capillary, $r$=16 μm. $C_0$=0.05%; $C_0$=0.1%; $C_0$=0.4%; $C_0$=0.5%; $C_0$=1%.

$\tau \sim R^2/D \approx 0.1$ s, if we use for estimations $R \sim 10$ μm and $D \sim 10^{-5}$ cm$^2$/s. A characteristic time scale of the spontaneous capillary imbibition into hydrophobic capillaries is around 100 s (see Fig. 13), while a characteristic time scale of the spontaneous capillary rise into hydrophobic capillaries is around $10^5$ s (see Fig. 14). Both time scales are much bigger than 0.1 s. The latter means that the surfactant concentration is constant in any cross section of the capillary and depends only on the position, $x$ (Fig. 12), that is, $C=C(t, x)$. We also assume that the adsorption equilibrium in any cross section is also reached. Taking this into account, the mass transfer of surfactant can be written as:

$$\frac{\partial (a+C)}{\partial t} = D\frac{\partial^2 C}{\partial x^2} + D_{SL}\frac{\partial^2 a}{\partial x^2} - v\frac{\partial C}{\partial x}, \quad 0<x<l(t) \tag{11}$$

where $D$ and $D_{SL}$ are diffusion coefficients of surfactant molecules in the volume and over the wetted capillary surface; $v=\mathrm{d}l/\mathrm{d}t$ is the meniscus velocity; and

$$a(x,t) = \begin{cases} \dfrac{2}{r}G_{SL}C(x,t) = F_{SL}C(x,t), & C<CMC \\ a_c = \dfrac{2}{r}G_{SL}C_c = F_{SL}C_c, & C>CMC \end{cases} \tag{12}$$

where $F_{SL}=(2/r)G_{SL}$.

### 3.2. Concentration below CMC

Let $C(x, t)$ and $a(x, t)$ be the local surfactant concentrations in the bulk solution and in the adsorbed state on the capillary surface, respectively. A constant surfactant concentration $C(0, t)=C_0<$CMC is kept at the capillary inlet. In this case, the surfactant transport in the filled portion of the capillary obeys Eq. (12). Substitution of Eq. (12) into Eq. (11) results in

$$(1+F_{SL})\frac{\partial C}{\partial t} = D_{ef}\frac{\partial^2 C}{\partial x^2} - \frac{\mathrm{d}l}{\mathrm{d}t}\frac{\partial C}{\partial x}, \quad 0<x<l(t) \tag{13}$$

where $D_{ef}=(D+F_{SL}D_{SL})$ is the effective diffusion coefficient. On the nonwetted portion of the capillary surface, $l(t)<x$, only surface diffusion takes place, that is:

$$\frac{\partial a}{\partial t} = D_{SV}\frac{\partial^2 a}{\partial x^2} \tag{14}$$

where $D_{SV}$ is the diffusion coefficient of surfactant molecules on the nonwetted hydrophobic capillary surface.

The following condition of the mass balance on the moving meniscus surface should be satisfied:

$$\left(D_{SV}\frac{\partial a}{\partial x}\right)_{l+} - \left(D\frac{\partial C}{\partial x} + D_{SV}\frac{\partial a}{\partial x}\right)_{l-} = (a_- - a_+)\frac{\mathrm{d}l}{\mathrm{d}t} \tag{15}$$

where $l_-$ and $l_+$ represent two points located on two opposite sides of the meniscus: on the liquid phase side, $l_-$, and on the unwetted side in front of the moving meniscus, $l_+$ (Fig. 12). Condition (15) expresses the conservation of mass at the moving meniscus and three-phase contact line.

We assume below the condition of a local equilibrium on the moving three-phase contact line. Using the latter condition, we conclude: $a_+ = \frac{a_-}{\exp(\Phi_+ - \Phi_-)}$. According to the previous, $\Phi_+$ is higher than $\Phi_-$, and hence, $a_+<a_-$.

Eqs. (13) and (14) with boundary condition (15) have a solution only if the concentration on the moving meniscus remains constant, that is, $C_m$=const. This corresponds to the experimentally observed law of the spontaneous imbibition, $l = K\sqrt{t}$, where $K$ is to be determined. The latter observation allows introducing a similarity variable $\xi = x/\sqrt{t}$. After that, the system under consideration can be directly solved and the following nonlinear algebraic equation for the determination of the concentration on the moving meniscus, $C_m$, can be deduced [6]:

$$\frac{K}{2}(F_{SL}-F_{SV}) = \frac{\left(\dfrac{C_0}{C_m}-1\right)D_{ef}\exp\left[\dfrac{(1-F_{SL})K^2}{4D_{ef}}\right]}{\displaystyle\int_0^K \exp\left[-\frac{(1+F_{SL})\xi^2}{4D_{ef}} + \frac{K\xi}{2D_{ef}}\right]\mathrm{d}\xi} - \frac{F_{SV}D_{SV}\exp\left[-\dfrac{K^2}{4D_{SV}}\right]}{\displaystyle\int_K^\infty \exp\left[-\frac{\xi^2}{4D_{SV}}\right]\mathrm{d}\xi} \tag{16}$$

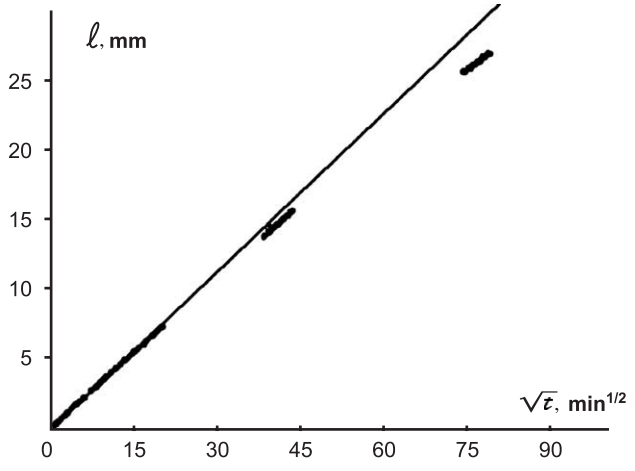


Fig. 14. Spontaneous capillary rise in a vertical hydrophobized quartz capillary ($r$=11 μm), Syntamid-5 surfactant solution ($C_0$=0.1%). Time evolution of the imbibition length, $l$ (mm), on time, $t$ (min).

The $K$ value governs the imbibition rate according to Eq. (5) and can be rewritten using Eq. (10) as

$$K = \sqrt{\frac{r\alpha(C_m - C_*)}{2\mu}} \tag{17}$$

Substitution of the latter equation into Eq. (16) gives the required equation for the determination of the unknown concentration on the moving meniscus, $C_m$.

Eqs. (16) and (17) give the solution of the problem under consideration. To solve Eq. (16), the following coefficients should be determined: diffusion coefficients, $D$, $D_{SL}$, and $D_{SV}$, adsorption constants, $G_{SL}$ and $G_{SV}$, capillary radius, $r$, solution viscosity, $\mu$, concentration at the capillary inlet, $C_0$, and the coefficient $\alpha$ in Eq. (17).

Numerical analysis of the final equation for $K$ shows that its value increases as $r$, $C_0$, $D$, and $D_{SL}$ increase or $D_{SV}$ decreases. The latter is due to the fact that the high surface mobility of the surfactant on the unwetted portion of the capillary reduces $C_m$ thereby inhibiting the imbibition.

### 3.3. Concentration above CMC

In the case of the surfactant concentration at the capillary inlet, $C_0$, above CMC, the diffusion and adsorption are accompanied by the destruction of the micelles. In this case, the total surfactant concentration, $C$, can be presented as $C=C_{mol}+C_M$, where $C_{mol}$ and $C_M$ are concentrations of free surfactant molecules and molecules inside micelles, respectively. Concentration of free molecules, $C_{mol}$, remains approximately constant above CMC and equal to CMC ($C_c$ below). The latter means that (i) a decrease in the surfactant concentration goes through disintegration of micelles, while the concentration of the free surfactant molecules remain constant, and (ii) the wetting stress depends on the concentration of the free molecules and hence remains independent of the concentration unless the concentration is below CMC: $\gamma(C_c)\cos\theta(C_c)=\Psi_c=\text{const}$. The latter means that the $K$ value, which determines the imbibition rate, is constant and is equal to:

$$K_c = \sqrt{r\alpha(C_c - C_*)/2\mu} = \text{const} \tag{18}$$

until concentration at the meniscus, $C_m$, is below CMC.

The value of $K_c$ for $C_0$>CMC~1% obtained in experiments with Syntamide-5 [6] corresponds to the contact angle $\theta_a$=89°, that is, only slightly different from 90°.

Unlike the case when the concentration at the capillary inlet is below CMC, the meniscus moves with velocity $l = K_c/\sqrt{t}$, where $K_c$ is given by Eq. (18) and does not vary with time. In this case, the surfactant adsorption on the capillary surface is accompanied by a continuous decrease of concentration, $C_m$, near the meniscus from $C_m=C_0$>CMC at the beginning of the imbibition process at $t$=0 to $C_m$=CMC or $C_m=C_c$ at the end of this first fast stage.

After $C_m$ reaches CMC, the condition $K_c$=const is no longer valid. The $K$ value decreases below $K_c$, and the imbibition rate slows down. After $C_m$=CMC is reached on the meniscus, a further reduction of concentration, $C_m$, causes separation of the micelle front (where $C$=CMC) from the meniscus surface. The micelle front movement is governed, as shown below, by the same law $l_M = K_M\sqrt{t}$, where $K_M<K$. The further stage of impregnation occurring when $C_m<C_c$ is described in the similar way to the previous section: the concentration no longer varies but remains *constant* and smaller than CMC.

The variations of the impregnation process associated with the above-mentioned phenomenon are illustrated in Fig. 13. A sharp change in the rate of impregnation at some distance $l=l_c$ is indeed observed for Syntamide-5 solutions at $C_0$>CMC.

Values of $l_c$, which correspond to the first fast stage of the imbibition process, are estimated below. As it is mentioned above, the first fast stage of the imbibition is determined by the dissociation of micelles close to the moving meniscus. Let us assume an adsorption of micelles on the meniscus according to Ref. [6], which is adopted according to the linear law $\Gamma=G_M(C_m-C_c)$, where $C_m-C_c$ is the micelles concentration at $C_0>C_c$ and $G_M$ is the corresponding adsorption constant. Diffusion of micelles is neglected below because of the short duration of the first stage. The mass balance on the moving meniscus during the first fast stage of the imbibition is:

$$(F_{SL} - F_{SV})C_c\frac{dl}{dt} = -G_M\frac{d(C_m - C_c)}{dt},$$
$$C_m(0) - C_c = C_0 - C_c \tag{19}$$

where $(F_{SL}-F_{SV})C_c$=const is the limiting adsorption on solid surface (micelles do not adsorb); the difference $C_m-C_c$ is equal to the micelle concentration. The left-hand side of Eq. (19) characterizes the surfactant adsorption rate on the newly wetted surface, and the right-hand side the micelle disintegration rate from the adsorbed layer of micelles.

The solution of Eq. (19) under the initial condition $t$=0, $C_m-C_c=C_0-C_c$ has the following form:

$$C_m(t) - C_c = (C_0 - C_c) - \frac{2C_c(G_{SL} - G_{SV})K_c\sqrt{t}}{rG_M} \tag{20}$$

The left-hand side of the latter equation vanishes as all the micelles near the meniscus disintegrate, i.e., the concentration $C_m$ reduces to CMC. Eq. (20) allows determining the instant $t=t_c$ when $C_m=C_c$. Using this condition and Eq. (20), the length of the fast imbibition can be determined as:

$$l_c = K_c\sqrt{t_c} = \left(\frac{C_0}{C_c} - 1\right)\frac{rG_M}{2(G_{SL} - G_{SV})} \tag{21}$$

For $r$~$2\times10^{-3}$ cm, $C_0$=2%, $C_c$=0.1%, and $l_c$=0.5 cm (in agreement with experimental observations), we get $G_M/(G_{SL}-G_{SV})$~25 in an agreement with Ref. [6].

The first fast stage of the imbibition is followed by the second slower stage. Now, concentration on the moving

meniscus, $C_m$, is below CMC. Two regions can be now identified inside the capillary: the first region, from the capillary inlet to some position, which we mark as $l_M(t)$, where concentration is above CMC and the solution includes both micelles and individual surfactant molecules, the second region, from $l_M(t)$ to $l(t)$, where concentration is below CMC and only individual molecules are transferred. The concentration is equal to CMC at $x=l_M(t)$. Consideration in the second region, $l_M(t)<x<l(t)$, is similar to that at concentration below CMC. That is why only the transport in the first region is considered below.

Inside the first region, $0<x<l_M(t)$, concentration of free surfactant molecules is constant and equal to CMC [6,7]. Hence, the transfer is determined by the diffusion of micelles and convection of all molecules. As it was mentioned above, the total concentration, $C=C_{mol}+C_M$, and $C_{mol}$ remains constant and equal to CMC, hence:

$$\frac{\partial C}{\partial t} = D_M \frac{\partial^2 C}{\partial x^2} - \frac{dl}{dt}\frac{\partial C}{\partial x} \tag{22}$$

where $D_M$ is the diffusion coefficient of micelles and $C=C_c+C_M$ is the total concentration. Adsorption on membrane pores is determined by the concentration of the free molecules, which is constant in the first region and so does the adsorption. It is the reason why the diffusion of adsorbed molecule in the first region is omitted in Eq. (22). Transfer of surfactant molecules is described by Eq. (13) in the second region (micelles-free region).

Boundary conditions on the moving boundary between the first and second regions, $l_M(t)$, are as follows:

$$D_M\left(\frac{\partial C}{\partial x}\right)_{x=l_M-} = D_{ef}\left(\frac{\partial C}{\partial x}\right)_{x=l_M+}, C(l_M,t) = C_c \tag{23}$$

As before, we assume that

$$l(t) = K\sqrt{t},\ l_M(t) = K_M\sqrt{t} \tag{24}$$

where $K$ is given by Eq. (17), that is, expressed via unknown concentration on the moving meniscus, $C_m$, and unknown constant $K_M$.

Afterwards, a similarity variable is introduced now in the same way as in the case of the concentration below CMC, that is, $\xi = x/\sqrt{t}$ in (Eqs. (13), (14), and (22). Using boundary conditions (17) and (23), a system of two nonlinear algebraic equations can be deduced with two unknown values, which are concentrations on the moving meniscus, $C_m$, and unknown constant $K_M$. It is necessary to remind that $K$ is express via $C_m$ according to Eq. (17) [6].

It is possible to show using the above-mentioned system that $K_M<K$, that is, the border between the first and the second regions moves slower than the meniscus [6]. The diffusion coefficient of micelles is much smaller than that of individual molecules. The latter means that the mentioned system of nonlinear algebraic equations includes a small parameter $D_M/D_{ef}\ll$ hence, constant $K$ only slightly differs from the same value in the case of concentration below CMC. That is, during second stage, the rate of the spontaneous imbibition is only slightly higher than in the case when concentration below CMC. Experimental data in Fig. 13 confirm this conclusion.

### 3.4. Spontaneous capillary rise in hydrophobic capillaries

A further confirmation of the adsorption of surfactant molecules in front of the moving meniscus on the bare hydrophobic substrate is a phenomenon of the spontaneous capillary rise of surfactant solutions in hydrophobic capillaries.

Let us consider a spontaneous capillary rise of surfactant solutions in hydrophobic capillaries. Fig. 14 shows the results of one of the capillary rise experiments with Syntamide-5 solution in a vertical hydrophobized quartz capillary [7]. The observed time evolution of the imbibition length, $l(t)$, follows $l(t)=K/\sqrt{t}$ dependency at the initial stage of the process. The value of $K$ determined from the slopes of the $l/\sqrt{t}$ dependencies corresponds to the advancing contact angle value, $\theta_a$, being only a few seconds less than 90°. At such $\theta_a$ values, the capillary rise would be expected to stop as soon as the liquid reached a height of $l_{max}=10^{-3}$ cm. However, it does not stop at this height but goes up to a height of 3–4 cm with almost constant $K$. The only explanation of this phenomenon is that the meniscus rises in the capillary following the surface diffusion front of surfactant molecules, which hydrophilise the bare hydrophobic capillary surface in front of the moving meniscus. At each position, $l$, the meniscus curvature must satisfy the following equilibrium condition:

$$\frac{2\Psi(C_m)}{r} = \rho g l(t) \tag{25}$$

where $\Psi(C_m)=\gamma(C_m)\cos\theta_a(C_m)$, $\rho$ is the density of the solution, and $g$ is the gravity acceleration. Since $\theta_a$ is very close to $\pi/2$ according to Eq. (10), we can use a linear dependency $\Psi(C_m)=\alpha(C_m-C_*)$.

Using Eq. (10), we can rewrite Eq. (25) as

$$l(t) = \frac{2\alpha}{\rho g r}(C_m - C_*) \tag{26}$$

During the initial stage of the capillary rise, $l(t) = K\sqrt{t}$ (see Fig. 14). The latter is possible only if $C_m = C_* + B\sqrt{t}$, and $B = K\frac{\rho g r}{2\alpha}$, where the constant $K$ is to be determined.

The latter equation shows that the case under consideration is governed by the completely different mechanism as compared with the case of the horizontal imbibition (where $C_m$ remains constant in time). In the case of the spontaneous capillary rise in hydrophobic capillaries, $C_m(t)$ does not remain constant but must increase as the capillary rise progresses. The comparison of Figs. 13 and 14 shows that the time scale of the spontaneous capillary rise is around 100 times bigger than the corresponding time scale in the case of the capillary imbibition into horizontal capillaries.

The maximum height of the capillary rise, $l_{max}$, is reached after the concentration on the meniscus, $C_m$,

becomes equal to the concentration at the capillary entrance, $C_0$. After that, the process stops. Using Eq. (26), $l_{max}$ is determined as

$$l_{max} = \frac{2\alpha}{\rho g r}(C_0 - C_*) \quad (27)$$

The latter means the experimental observation presented in Fig. 14 corresponds to $l(t) \ll l_{max}$, that is, the initial stage of the capillary rise.

Below, the problem of the spontaneous capillary rise of surfactant solutions in hydrophobic capillaries is considered in the case when concentration at the capillary inlet is below CMC. In this case, the transport of surfactant molecules is described by Eqs. (13) and (14) and boundary condition (15). The substantial difference from the spontaneous capillary imbibition is that now the relation between $l(t)$ and concentration on the moving meniscus, $C_m$, is given by relation (26), which shows that $C_m$ is an unknown function of time. Using these equations and boundary conditions, we show below that $l(t)$ dependency on time can be calculated and it is proportional to square root of time at the initial stage of the capillary rise (see Ref. [7] for details).

Solution in Ref. [7] shows that at the initial stage of the capillary rise, $l(t)$ develops as

$$l(t) = K\sqrt{t},\ K = l_{max}\sqrt{\frac{2\kappa}{\omega}} \quad (28)$$

where $\kappa$ and $\omega$ are defined as follows

$$\omega = \frac{C_*}{C_0 - C_*},\ \kappa = \frac{\lambda}{2+\chi}, \lambda = \frac{4D_{ef}(1+F_{SL})}{3\Delta F F_{SV} l_{max}^2},$$
$$\chi = \frac{2\Delta F C_0}{F_{SV}(C_0 - C_*)}$$

The latter dependency agrees with experimental observations in Ref. [6] (see Fig. 14). At the final stage of the capillary rise, $l(t)$ levels off as

$$l(t) = l_{max}\left(1 - \frac{\omega + 1}{\kappa t}\right)$$

According to Eq. (27) and Fig. 11, $l_{max}^{exp}$~35 mm in the experiment presented in Fig. 14. Experimental value of, $K^{exp}$, in Eq. (28), calculated according to Fig. 14 is $K^{exp} \sim 5\times10^{-3}$ cm/s$^{1/2}$. In experiments presented in Fig. 14, $\omega$~1. The comparison of the latter estimations gives $\kappa \sim 10^{-5}$ s$^{-1}$, which coincide with the theoretical value, if we assume that $F_{SV} \ll F_{SL}$, $D \sim 10^{-5}$ cm$^2$/s, and use estimation $G_{SL} \sim 10^{-5}$ cm [6] and value of $\alpha$ is taken directly from Fig. 11.

## 4. Imbibition of surfactant solutions into porous substrates: partial wetting case

Kinetics of the capillary imbibition of aqueous surfactant solutions into hydrophobic capillaries has been investigated earlier in Section 3. It has been shown that the rate of imbibition is controlled by the adsorption of the surfactant molecules in front of the moving meniscus on the bare hydrophobic surface of the capillary. This process results in a partial hydrophilisation of the surface of the capillary in front of the moving meniscus and gives a possibility to penetrate into the initially hydrophobic capillary. That is, no surfactant molecules on the meniscus—no imbibition. Below, the imbibition of surfactant solutions into the porous substrates, which are partially wetted by water, is considered. It is shown that situation in this case is considerably different from the case of hydrophobic porous media.

### 4.1. Theory

The imbibition of aqueous surfactant solutions into a single cylindrical capillary, those walls are partially wetted by water, is considered below. A single capillary is used as a model of a porous medium.

The situation in this case is different from the case of hydrophobic capillaries (Section 3): water can penetrate into the capillary even in the absence of surfactant molecules on the moving meniscus. However, presence of surfactant molecules on the moving meniscus results in a lower contact angle (as compared with the pure water) and hence in a higher capillary pressure behind the meniscus. As a result, the imbibition rate increases with concentration of surfactant molecules on the moving meniscus.

The moving meniscus covers fresh parts of the capillary walls, where surfactant molecules have not adsorbed yet. This means that the imbibition process is accompanied by the simultaneous adsorption of surfactant molecules onto fresh parts of the capillary walls in a vicinity of the moving meniscus. The adsorption is reversibly proportional to the radius of the capillary, that is, the thinner the capillary, the higher the adsorption. On the other hand, the rate of the imbibition is lower in thinner capillaries (higher friction). The latter gives more time to diffusion to bring new surfactant molecules and cover the fresh part of the capillary walls. That is, there are two competing opposite trends. This means if the capillary radius is smaller than some critical value, then adsorption goes faster than the imbibition process, all surfactant molecules are adsorbed on the capillary walls, that is, nothing is left for the meniscus, and the concentration on the moving meniscus remains zero. This qualitative consideration shows that if capillary radius is smaller than some critical value, then the rate of the imbibition of surfactant solutions remains independent of the surfactant concentration in the feed solution and equals to that of the pure water.

This qualitative conclusion is justified below using theoretical consideration of the capillary imbibition of aqueous surfactant solutions into cylindrical capillaries; those walls are partially wet by water.

Let us consider an imbibition of surfactant solution from a reservoir with a fixed surfactant concentration, $C_0$ (feed solution), into a thin capillary with radius $r \ll L$ (Fig. 12), where $L$ is the capillary length. The capillary walls are

partially wet by pure water (at zero concentration of surfactant), that is,

$$\gamma(0)\cos\theta_a(0) = \gamma_{SV}(0) - \gamma_{SL}(0) > 0 \quad (29)$$

where $\gamma$, $\gamma_{SV}$, $\gamma_{SL}$, and $\theta_a$ are the liquid–air, the solid substrate–vapor, the solid substrate–liquid interfacial tensions, and the advancing contact angle, respectively. All these values are concentration-dependent. Let $C_m$ be the bulk concentration of surfactant behind the moving meniscus. Then

$$\gamma(C_m)\cos\theta_a(C_m) = \gamma_{SV}(0) - \gamma_{SL}(C_m) > \gamma_{SV}(0) - \gamma_{SL}(0) = \gamma(0)\cos\theta_a(0) \quad (30)$$

It is assumed that the imbibition process in the case under consideration goes sufficiently fast and transfer of the surfactant molecules on the bare surface in front of the moving meniscus can be neglected because this process goes much slower (see Section 3). Hence, the solid–vapor interfacial tension, $\gamma_{SV}$, does not depend on the surfactant concentration and remains equal to its value at zero concentration. It is also taken into account in Eq. (30) that $\gamma_{SL}(C_m)$ is a decreasing function of the surfactant concentration. Eq. (30) shows that $\Psi(C_m)=\gamma(C_m)\cos\theta_a(C_m)$ is an increasing function of the concentration, with the maximal value, $\Psi_{max}=\Psi(C_{CMC})$, reached at CMC and the minimal value, $\Psi_{min}=\gamma_{SV}(0)-\gamma_{SL}(0)$, reached at the zero surfactant concentration.

### 4.2. Concentration below CMC

Let the surfactant concentration at the capillary entrance be below CMC, $C_0$<CMC. The transfer of surfactant molecules in the filled portion of the capillary is described by the convective diffusion Eq. (14) as in Section 3.

As a result of adsorption on the capillary wall, the concentration of the surfactant molecules on the moving meniscus, $C_m$, is lower than at the capillary entrance and should be determined in a self-consistent way.

Solution of Eq. (14) should be subjected with the following boundary condition at the moving meniscus Eq. (15), where adsorption in front of the moving meniscus is neglected:

$$\frac{2\Gamma(C_m)}{R}\frac{d\ell}{dt} = -D\left.\frac{\partial C}{\partial x}\right|_{x=\ell(t)} \quad (31)$$

The latter condition expresses the conservation of mass at the moving meniscus and the three-phase contact line.

Because of $r \ll L$, the liquid flow inside the capillary is the simple Poiseuille flow; that means

$$\frac{dl}{dt} = \frac{r^2}{8\mu}\frac{2\gamma(C_m)\cos\theta_a(C_m)}{r}\frac{1}{l} = \frac{r\gamma(C_m)\cos\theta_a(C_m)}{4\mu l}$$

where $\mu$ is the dynamic viscosity, which is assumed to be independent of surfactant concentration. It is assumed below that the surfactant concentration remains constant at the moving meniscus (similar to the case of hydrophobic capillaries in Section 3). Solution of the latter equation using initial condition $l(0)=0$ gives

$$l(t) = K\sqrt{t},\ K = \sqrt{\frac{r\gamma(C_m)\cos\theta_a(C_m)}{2\mu}} \quad (32)$$

Substitution of Eq. (32) into Eq. (14) results in

$$\frac{2}{r}\frac{\partial\Gamma}{\partial t} + \frac{\partial C}{\partial t} = D\frac{\partial^2 C}{\partial x^2} - \frac{K}{2\sqrt{t}}\frac{\partial C}{\partial x} \quad (33)$$

with boundary condition

$$\frac{\Gamma(C_m)K}{K\sqrt{t}} = -D\left.\frac{\partial C}{\partial x}\right|_{x=K\sqrt{t}} \quad (34)$$

To further simplify the mathematical treatment of the problem under consideration, the simplest adsorption isotherm is adopted below:

$$\Gamma(C) = \begin{cases} \Gamma_\infty, & C>0 \\ 0, & C=0 \end{cases} \quad (35)$$

It is worth mentioning that according to Eq. (30), $\Psi$ in the case under consideration is independent of the concentration and equal to its maximal value, $\Psi_{max}$. Solution of problems (33) and (34) is given in Ref. [9], which yields the following expression for the concentration on the moving meniscus:

$$C_m = C_0 - \Gamma_\infty\sqrt{\frac{\pi\Psi_{max}}{2D\mu r}} \quad (36)$$

The concentration on the moving meniscus should be positive, $C_m>0$, that is, the following requirement should be satisfied:

$$C_0 > \Gamma_\infty\sqrt{\frac{\pi\Psi_{max}}{2D\mu r}} \quad (37)$$

or

$$r > \frac{\Gamma_\infty^2\pi\Psi_{max}}{2D\mu C_0^2} \quad (38)$$

Let us introduce the following notation

$$r_{cr} = \frac{\Gamma_\infty^2\pi\Psi_{max}}{2D\mu C_{CMC}^2} \quad (39)$$

Two cases are considered below: (i) $r<r_{cr}$ and (ii) $r>r_{cr}$.

In the first case, (i), condition (38) is violated at any concentrations in the feed solution between zero and CMC. This means that concentration of surfactant molecules on the moving meniscus is equal to zero at any concentration from this range. Hence, there are two regions behind the moving meniscus: in the first region, close to the capillary entrance, the concentration is changing from $C_0$ in the feed solution to zero on the moving border between two regions; the first region is followed by the second region where concentration

remains zero over duration of the whole process. The moving border between these two regions is [9]

$$\ell_1(t) = K(1-\lambda\chi)\sqrt{t},\ \chi = \left(\frac{\Gamma_\infty}{C_0}\sqrt{\frac{2\pi\Psi_{\min}}{D\mu r}}\right)^{1/2} \quad (40)$$

In this case, the concentration on the meniscus remains zero and the meniscus moves "slowly" according to Eq. (32), $l(t) = \sqrt{\frac{r\Psi_{\min}}{2\eta}}\sqrt{t}$.

The main conclusion from this consideration is that the adsorption process in sufficiently thin capillaries consumes all surfactant and the imbibition is not influenced by the presence of surfactants in the feed solution at any concentration.

Let us consider the second case when the capillary radius is bigger than the critical value determined by Eq. (38), that is, $r>r_{cr}$.

If concentration in the feed solution is low enough, that is, condition (38) is violated, then the concentration on the moving meniscus, $C_m$, is equal to zero and meniscus moves "slowly" according to Eq. (38). It is worth noticing that the capillary radius is assumed to be bigger than in the previous case.

If, however, concentration in the feed solution, $C_0$, is high enough, that is, condition (37) is satisfied, then concentration of the surfactant molecules is different from zero on the moving meniscus and the imbibition process goes "faster" according to $l(t) = \sqrt{\frac{r\Psi_{\max}}{2\eta}}\sqrt{t}$.

Hence, if the capillary radius is bigger than the critical value, then the whole concentration range in the feed solution can be subdivided into two parts: low concentration range $C_0<C_{cr} = \Gamma_\infty\sqrt{\frac{\pi\Psi_{\max}}{2D\eta r}}$, when the adsorption consumes all surfactant molecules and the concentration on the moving meniscus is equal to zero and meniscus moves "slowly"; and high concentration range $C_0>C_{cr} = \Gamma_\infty\sqrt{\frac{\pi\Psi_{\max}}{2D\eta r}}$, when the adsorption does not consume all surfactant molecules and the concentration on the moving meniscus is different from zero, meniscus moves "fast".

### 4.3. Concentration above CMC

If the concentration in the feed solution, $C_0$, is above CMC, then after some short initial period inside the capillary, two zones form (Section 3): in the first region, close to the capillary entrance, concentration inside the capillary is higher than CMC; this region is followed by the second region where concentration is below CMC. The concentration is equal to CMC at the border between these two regions. Consideration similar to that in Section 3 and presented above shows that the main conclusion remains unchanged in this case: there is a critical radius of the capillary below which concentration on the moving meniscus remains zero at any concentration in the feed solution.

In the same way as in Section 3, a system of two nonlinear algebraic equations can be deduced for determination of two unknown values: the concentration on the moving meniscus, $C_m$, and the position of the boundary, $K_M$, where concentration is equal to CMC. This system include a small parameter, which the ratio of diffusion coefficients of micelles and free surfactant molecules, $D_M/D \ll 1$. Using this new small parameter, it is possible to show that the solution of the mentioned system only slightly deviates from the solution in the previous case when concentration is below CMC.

The latter means that the constant $K$ and the expression for the critical radius (38) is only slightly different from the same value in the case of concentration below CMC. Hence, the previous conclusion concerning the existence of the critical radius remains valid even at concentrations above CMC, which is confirmed below by experimental data.

Rectangular membrane samples 1.5×3 cm were used. Those porous samples were cut from the Cellulose Nitrate membranes purchased from Millipore. Three different membranes with averaged pore size 0.22, 0.45, and 3.0 μm were used. Each membrane sample was immersed on 0.1–0.2 cm into a liquid container, and the position of the imbibition front was monitored over time.

It was checked [9] that in all experimental runs, the gravity action could be neglected. A unidirectional flow of liquid inside the porous substrate took place. Using Darcy's law, we can conclude that $d^2(t)=kp_c t/\mu$, where $\ell(t)$ now is the position of the imbibition front inside the porous layer, $k$ is the permeability of the porous membrane, and $p_c$ is an effective capillary pressure inside the porous sample. The permeability of the porous layer and the capillary pressure enters as a product in the latter equation, that is, as a single coefficient. Experiments were carried out to determine this coefficient and its dependency on the surfactant concentration if any. It was found that in all runs, $d^2(t)/2$ proceeds along a straight line, whose slope gives us $kp_c$ value.

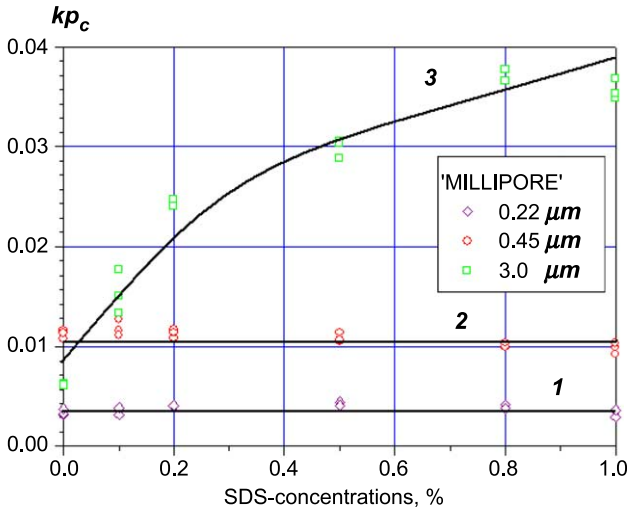


Fig. 15. $kp_c$ dependency on concentration of SDS solutions for nitrocellulose membranes with different averaged pore sizes. Remains constant in the case of membranes with averaged pore size of 0.22 μm (line 1) and 0.45 μm (line 2). Increases with surfactant concentration in the case of membrane with averaged pore size 3 μm (curve 3 is drawn simply to guide eyes).

According to our previous notations $kp_c=K^2\eta$.

Fig. 15 presents $kp_c$ dependency on the concentration of the SDS in the feed solution for three different membranes. It was found that $kp_c$ values are independent of concentration in the case of membranes with 0.22 and 0.45 μm averaged pore size. However, in the case of membranes with 3.0-μm averaged pore size, $kp_c$ increases with SDS concentration. The latter means that the critical radius, $R_{cr}$, is somewhere in between 0.45 and 3.0 μm. Fig. 15 confirms the conclusion concerning the existence of the critical pore radius below which permeability is independent of surfactant concentration.

## 5. Spreading of surfactant solutions over hydrophobic substrates

Surfactant adsorption on solid–liquid and liquid–vapor interfaces changes the corresponding interfacial tensions. Liquid motion caused by the surface tension gradient on a liquid–vapor interfaces (Marangoni effect) is the most investigated process [8]. The phenomena produced by the presence of surfactant molecules on a solid–vapor interface have been studied less. In Section 3, the imbibition of surfactant solutions into thin quartz capillaries was investigated. In the present section, we address the problem of aqueous surfactant solutions spreading over hydrophobic surfaces from both the theoretical and experimental points of view.

### 5.1. Theory

Let a small water drop be placed on a hydrophobic surface. If the drop is small enough, then the effect of gravity can be ignored. Accordingly, the drop radius $r$ has to be smaller than the capillary length, $a$, and hence, $r\le a=\sqrt{\frac{\gamma}{\rho g}}$, where $\rho$ and $\gamma$ are the liquid density and liquid–vapor interfacial tension, respectively, and $g$ is the gravity acceleration.

Let us assume that in the absence of surfactant, the drop forms an equilibrium contact angle bigger than $\pi/2$. If the water contains surfactants, then the following three transfer processes take place from the liquid onto all three interfaces: surfactant adsorption at both (i) the inner liquid–solid interface and (ii) the liquid–vapor interface, and (iii) transfer from the drop onto the solid–vapor interface just in front of the drop. Adsorption processes (i) and (ii) result in a decrease of corresponding interfacial tensions, $\gamma_{SV}$ and $\gamma$. The transfer of surfactant molecules onto the solid–vapor interface in front of the drop results in an increase of a local free energy; however, the total free energy of the system decreases. That is, surfactant molecule transfer (iii) goes via a relatively high potential barrier and hence goes considerably slower than the adsorption processes (i) and (ii). Hence, they are "fast" processes as compared with the third process (iii).

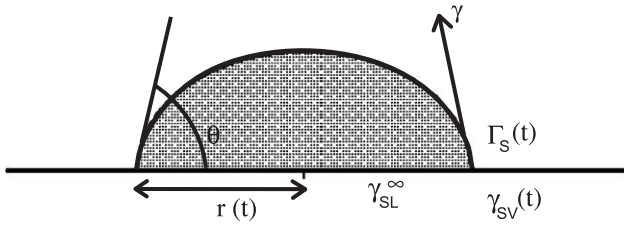


Fig. 16. Sketch of the geometry of a drop placed on a solid substrate.

The transfer of surfactant molecules onto the unwetted (hydrophobic) solid–vapor interface in front of the liquid has been shown in Section 3 to play an important role in the wetting of hydrophobic surfaces.

All three surfactant transfer processes are favorable to spreading, as they result in both an increase of the spreading power, $\gamma_{SV}-\gamma-\gamma_{SL}$, and hence a decrease of the contact angle (Fig. 16). As it was mentioned above, the transfer of surfactant molecules from the drop onto the solid–vapor interface in front of the drop results in an increase of local surface tension, $\gamma_{SV}$. Hence, it is the slowest process that will be the rate-determining step. Let us define the initial contact angle as

$$\cos\theta^0=\frac{\gamma_{SV}^0-\gamma_{SL}^\infty}{\gamma}\le\frac{\pi}{2}, \tag{41}$$

where $\gamma_{SV}^0$ is the initial values of solid–vapor interfacial tension, $\gamma_{SL}^\infty$ and $\gamma$ are solid–liquid and liquid–vapor interfacial tensions, respectively, which already reached their equilibrium values because the adsorption process on the liquid–vapor and solid–liquid interfaces has been completed (they are fast processes); the solid–vapor interface still has its initial value on a bare hydrophobic interface without any surfactant adsorption. At this «initial» instant of time, a process of slow transfer of surfactant molecules starts from the drop onto the solid–vapor interface. Let $\Gamma_S(t)$ be the instantaneous value of surfactant adsorption onto the solid surface in front of the liquid drop on the three phase contact line and $\Gamma_e$ be the equilibrium surface density of adsorbed surfactant molecules, which would eventually be reached. The driving force of the process is proportional to the difference $\Gamma_S(t)-\Gamma_e$. Hence, the surfactant adsorption behaviour with time is described by

$$\frac{d\Gamma_S(t)}{dt}=\frac{1}{\tau_s}[\Gamma_e-\Gamma_S(t)] \tag{42}$$

with the initial condition

$$\Gamma_S(0)=0\ at\ t=0 \tag{43}$$

where $\tau_S$ is the time scale of surfactant transfer from the drop onto the solid–liquid interface at three-phase contact line. Let us assume that

$$\frac{1}{\tau_S}=\frac{1}{\tau_T}\Xi\exp\left(\frac{-\Delta E}{kT}\right) \tag{44}$$

where the prefactor $1/\tau_T$ is determined by thermal fluctuations only; $\Delta E$ is an energy barrier for surfactant transfer from the liquid drop onto the solid–liquid interface; $k$ and $T$ are Boltzmann's constant and absolute temperature, respectively; $\Xi$ is a fraction of the drop liquid–vapor interface covered with surfactant molecules. Obviously, surfactant molecules position on a hydrophobic interface is "hydrophobic tails down."

It has been assumed in Eq. (44) that transfer of surfactant molecules onto the hydrophobic solid interface takes place only from the liquid–vapor interface. It is difficult to assess the contribution of surfactant molecule transfer along the solid surface from beneath the liquid. However, experimental data below support this assumption (although they do not prove it decisively). The drop surface coverage $\Xi$ is an increasing function of the bulk surfactant concentration inside the drop, whose maximum is reached close to the CMC. It follows from Eq. (44) that $\tau_S$ should decrease with an increase of the concentration at low surfactant concentrations inside the drop, while $\tau_S$ should level off and reach its lowest value above the CMC. Both of these effects are observed in experimental results (compare Fig. 18).

As the drop adopts a position according to the triangle rule, the contact angle, $\theta(t)$, is determined by the relationship

$$\cos\theta(t) = \frac{\gamma_{SV}(t) - \gamma_{SL}^{\infty}}{\gamma} \tag{45}$$

where $\gamma_{SV}(t)$ is the instantaneous solid–vapor interfacial tension at the three-phase contact line. The latter dependency is determined by $\Gamma_S(t)$. According to Antonov's rule

$$\gamma_{SV}(t) = \gamma_{SV}^{\infty}\frac{\Gamma_S(t)}{\Gamma^{\infty}} + \gamma_{SV}^{0}\left(1 - \frac{\Gamma_S(t)}{\Gamma^{\infty}}\right) \tag{46}$$

where $\gamma_{SV}^{\infty}$ is the solid–vapor interfacial tension of the surface completely covered by surfactants and $\Gamma^{\infty}$ is the total number of sites available for adsorption. Hence, the final value of the contact angle can be determined from Eq. (45) as

$$\cos\theta^{\infty} = \frac{\gamma_{SV}^{\infty} - \gamma_{SL}^{\infty}}{\gamma} \tag{47}$$

According to Eq. (46), solid–vapor interface in front of the spreading drop changes its wettability with time: from a highly hydrophobic at the initial stage to a partially hydrophilic at the final stage.

Substitution of Eq. (46) in Eq. (45) yields the instantaneous contact angle

$$\cos\theta(t) = \cos\theta^{0} + \lambda\frac{\Gamma_S(t)}{\Gamma^{\infty}} \tag{48}$$

where $\cos\theta^0$ is given by Eq. (41), and the positive value of $\lambda$ is $\lambda=(\gamma_{SV}^{\infty}-\gamma_{SV}^{0})/\gamma$.

Eq. (42) with initial condition (43) yields the following solution

$$\Gamma_S(t) = \Gamma_e(1 - \exp(-t/\tau_S)) \tag{49}$$

Using Eq. (49) in Eq. (48) gives the final expression for the instantaneous contact angle

$$\cos\theta(t) = \cos\theta^{0} + \lambda\frac{\Gamma_e}{\Gamma^{\infty}}(1 - \exp(-t/\tau_S)) \tag{50}$$

A simple geometrical consideration (Fig. 16) shows that the radius of the wetted spot, $r(t)$, occupied by the drop can be expressed as

$$r(t) = \left(\frac{6V}{\pi}\right)^{1/3}\frac{1}{\left[\tan\frac{\theta}{2}\left(3 + \tan^2\frac{\theta}{2}\right)\right]^{1/3}} \tag{51}$$

where $V$ is the drop volume, which is supposed to remain constant, and the contact angle, $\theta$, is given by Eq. (50).

Eqs. (50) and (51) include two parameters: the dimensionless $\beta=\lambda\Gamma_e/\Gamma^{\infty}$ and the time scale $\tau_S$. It follows from Eq. (50) that $\beta=\cos\theta^{\infty}-\cos\theta^{0}>0$, where $\theta^{\infty}$ is the contact angle after the spreading process, is completed. Both values of the contact angle, $\theta^0$ and $\theta^{\infty}$, have been measured and hence $\beta$ can be determined experimentally. Only $\tau_S$ was used to fit the experimental data [10].

Two types of substrate were used, a PTFE film and a polyethylene (PE) wafer in [10] to monitor spreading of aqueous surfactant drops. The equilibrium macroscopic contact angles obtained were 105° and 90° for PTFE and PE substrates, respectively (for pure water droplets).

Aqueous solutions of sodium dodecyl sulfate (SDS) from Merck with weight concentrations from 0.005% up to 1% (the CMC of the SDS is 0.2%) were used in spreading experiments [10].

According to experimental observations [10], all the spreading drops were of spherical shape; no disturbances or instabilities were detected. Immediately after deposition, the drops had a contact angle, which differs slightly from the equilibrium angle of pure water on the same substrate. After a very short initial time, the drops reached a position which is referred to as "the initial" position. After that, for 1–15 s,

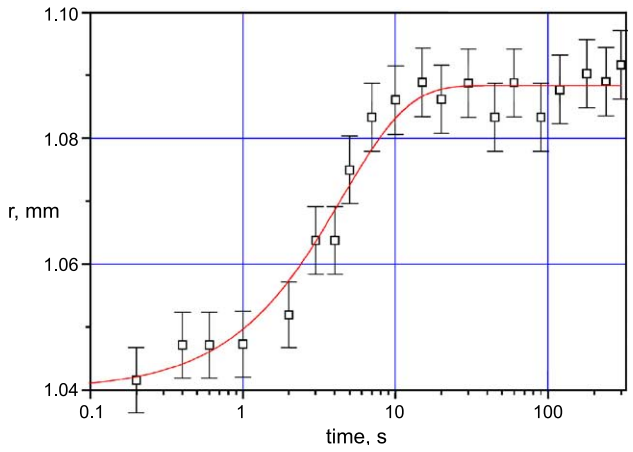


Fig. 17. Time evolution of the spreading of a water drop (aqueous solution $c$=0.05% SDS; 2.5±0.2 μl volume) over PTFE wafer. Error bars correspond to the error limits of video evaluation of images (pixel size).

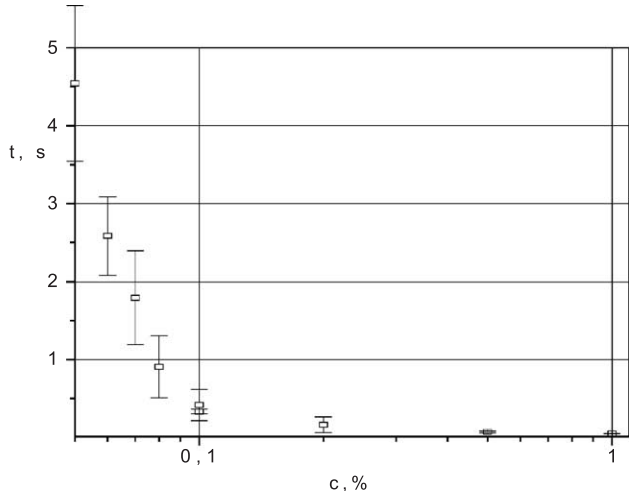


Fig. 18. Fitted dependency of $\tau_s$ on surfactant concentration inside the drop (spreading over PTFE wafer). Error bars correspond to the experimental points scattering in different runs; squares are average values.

depending on the SDS concentration, drops remained at the initial position. Then drops started to spread until a final value of the contact angle was reached and the spreading process was completed.

In Fig. 17, the evolution of the spreading radius of a drop over PTFE film at 0.05% SDS concentration is plotted. The solid line corresponds to the fitting of the experimental data using Eqs. (50) and (51), with $\tau_S$ used as a fitting parameter.

Fig. 18 shows that qualitatively, the $\tau_S$ dependency agrees with the theoretical prediction and tends to support the assumption concerning the mechanism of surfactant molecule transfer onto the hydrophobic surface in front of the drop.

Similar results were obtained for the spreading over the polyethylene substrate for concentrations below CMC. However, in this case, the spreading behaviour of drops at concentrations above CMC differs with increasing SDS concentration [10]. The rate of a spreading is increased so much that at 1% concentration, the power law with the exponent 0.1 fits experimental data reasonably well. This clearly shows a transition to a different mechanism of spreading, which can be understood in the following way. In the previous considerations, the influence of the viscous forces was ignored. It was assumed that $\tau_S \gg \tau_{vis}$, where $\tau_{vis}$ is a time scale of viscous spreading. In the latter case, $\tau_S$ decreases so considerably that mentioned inequality becomes invalid and now rather $\tau_S \sim \tau_{vis}$ becomes valid.

## 6. Spreading of aqueous droplets induced by overturning of amphiphilic molecules or their fragments in the surface layer of an initially hydrophobic substrate

In recent years, a large number of researches have been published (see, for example, Refs. [11–14] and relevant references therein) demonstrating that interaction of a polymer with a polar liquid (first of all, with water and aqueous solutions) may result in the spontaneous rearrangement ("self-organization") of its surface layer, providing the minimization of the interfacial free energy due to the emergence (or adsorption) of polar groups at the surface. Depending on the structure of the polymer macromolecules, the physical state of the polymer, and other factors, such a rearrangement may involve various forms of molecular motion, from the reorientation of individual amphiphilic side groups (when their rotation around the backbone is allowed) to the diffusion of macromolecules as a whole. Each of these processes may occur on different time scales. If the characteristic time scale of self-organization is comparable with the time of measurement, this process may be observed while studying the contact angle (and size) of an aqueous droplet on time of contact with polymer [15]. Such a "prolonged" spreading of aqueous droplets occurs also during the study of the wettability of model systems such as apolar polymers containing low-molecular-weight amphiphilic additives (surfactants) capable of adsorption and/or reorientation at the polymer–liquid interface [15].

Langmuir was the first to mention the possible reorientation ("overturning") of amphiphilic molecules in contact with a polar liquid [16]. Later, experimental data were obtained that demonstrated the occurrence of such process in monolayers and Langmuir–Blodgett films composed of long-chain fatty acids [17] and at the surface of mixtures of such acids with paraffin [18] during contact with an aqueous droplet, resulting in gradual droplet spreading. Recently, such a situation has also been observed for the spreading of a droplet over the surfaces of polymers, when the amphiphilic groups of their macromolecules are capable of reorientation by rotating around the macromolecule backbone.

Preliminary, the rate of spreading was analyzed in terms of formal chemical kinetics [17,18], and the mechanism of the process (the dynamic situation in the vicinity of the three-phase contact line) was not considered.

The aim of this section is to analyze the mechanism of the spontaneous spreading of a droplet of aqueous droplets induced by the overturning of amphiphilic molecules (or their fragments) in the surface layer of a solid substrate and to develop a quantitative theory describing this process.

### 6.1. Derivation of basic equations

Let us consider the spreading of an aqueous droplet over a solid substrate ignoring the evaporation of the liquid, i.e., assuming that the droplet volume remains constant during spreading. It is assumed also that the substrate is smooth, horizontal, and (what is important for the further discussion) contains in the surface layer rotationally mobile amphiphilic molecules (or amphiphilic fragments of molecules; for brevity, we hereafter mention only molecules) capable of overturning in the plane perpendicular to the surface and incapable of lateral motions in the plane of the substrate.

Hence, each of the amphiphilic molecules may be in one of two states: (i) non-overturned ("normal"), i.e., when the hydrophilic head group of the molecule is oriented downward into the substrate while the hydrophobic "tail" is directed upward into the second phase (air or water) in contact with the substrate; and (ii) overturned state, i.e., in the opposite (as compared to the previous case) orientation of hydrophilic and hydrophobic moieties of the molecule (Fig. 19).

Let $N_\infty$ and $N$ be the total number of amphiphilic molecules per surface area of the substrate capable of overturning and the number of overturned molecules, respectively; then $p=N/N_\infty$ is the probability to find an overturned molecule. Let us consider the process of transition of a system to the equilibrium state during the contact of the substrate surface with the air, provided that initially, the system was somehow disturbed from an equilibrium state.

Let us consider for simplicity a linear chain of amphiphilic molecules because a switch to the two-dimensional case will be self-evident. Let $p_i(t)$ be the probability of the occurrence of molecule $i$ at the instant $t$ in the overturned state; then the same probability at the time $t+\Delta t$ will be equal to:

$$p_i(t+\Delta t) = p_i(t) + P_V\Delta t - P_{SV}\Delta t + P_d\Delta t - P_b\Delta t \qquad (52)$$

where $P$ with subscripts are the probabilities of direct and reverse overturnings per unit time: $P_V$ is the overturning probability caused by the interaction with the air of the amphiphilic molecule that has not been overturned previously; $P_{SV}$ is the overturning probability caused by the interaction with underlying molecules of the molecule that was overturned previously; and $P_d$ and $P_b$ are the probabilities corresponding to the direct and the reverse overturnings of a molecule due to its interaction with neighbouring molecules. Only the interactions with the nearest neighbours are accounted for, i.e., with the molecules having numbers $i+1$ and $i-1$.

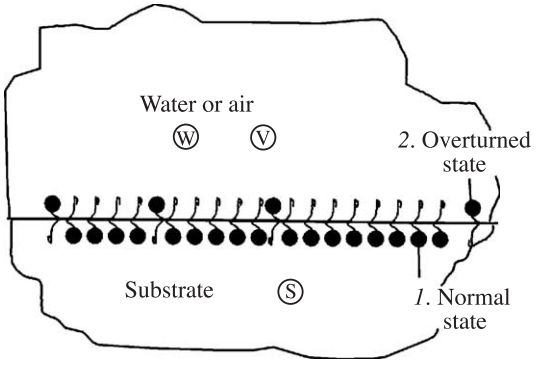


Fig. 19. Polymeric substrate containing rotationally mobile amphiphilic chains in contact with air or water. *V*—air, *W*—water, *S*—polymeric substrate. 1—amphiphilic chains in the "normal" state, 2—amphiphilic chains in the overturned state.

All the probabilities in Eq. (52) may be written in the following form:

$$\begin{aligned} P_V &= \alpha_V(1-p_i),\\ P_{SV} &= \alpha_{SV}p_i\\ P_d &= \beta[p_{i-1}(1-p_i)+p_{i+1}(1-p_i)]\\ P_b &= \beta[(1-p_{i-1})p_i+(1-p_{i+1})p_i] \end{aligned} \qquad (53)$$

where constants $\alpha_V$, $\alpha_{SV}$, and $\beta$ entering into the definitions of probabilities in Eq. (53) have the dimensionality of reciprocal time and are determined below using the energy of molecular interaction with surrounding phases in overturned and non-overturned states:

$$\alpha_V = \alpha\exp[-\Re_V] \qquad (54)$$

$$\alpha_{SV} = \alpha\exp[\Re_V] \qquad (55)$$

$$\beta = \alpha[\exp(\chi)-1] \qquad (56)$$

where $\chi = z\frac{2U_{th}-U_{tt}}{RT}$, $\Re_V = \frac{U_{ts}+U_{hv}-U_{tv}-U_{hs}}{RT}$; subscripts t, h, v, and s correspond to the hydrophobic tail of a molecule, to its hydrophilic head group, to the air, and to the underlying molecules of the substrate, respectively; $\alpha$ denotes the corresponding values in the absence of any interaction, i.e., determined only by thermal fluctuations; and $z$ is the number of neighbouring molecules, i.e., $z=2$ for a linear chain and $z=4$ for the two-dimensional case. It follows from definitions (54) and (55) that $\alpha_V \ll \alpha_{SV}$.

Let us consider Eq. (56) in more detail. If expressions (54) and (55) involve both overturnings due to the thermal fluctuations and those caused by the interaction with the surrounding media, then, in contrast to these expressions, Eq. (56) involves only the overturnings related to the interactions between the neighbours; hence, random overturnings caused by thermal fluctuations should not be taken into account because they do not result in the transfer of the overturned state. It is the reason why the unity is subtracted in Eq. (56).

Substituting expressions (53)–(56) into Eq. (52) yields:

$$\begin{aligned} \frac{p_i(t+\Delta t)-p_i(t)}{\Delta t} &= \alpha_V[1-p_i(t)] - \alpha_{SV}p_i(t)\\ &\quad + \beta\{[p_{i-1}(t)+p_{i+1}(t)][1-p_i(t)]\\ &\quad - [2-p_{i-1}(t)-p_{i+1(t)}]p_i(t)\} \end{aligned}$$

Taking the limit in the last expression at $\Delta t \to 0$ results in:

$$\begin{aligned} \frac{dp_i(t)}{dt} &= \alpha_V[1-p_i(t)] - \alpha_{SV}p_i(t)\\ &\quad + \beta[p_{i+1}(t)+p_{i-1}(t)-2p_i(t)] \end{aligned} \qquad (57)$$

Let $a$ be the mean distance between molecules capable of overturning. Then Eq. (57) may be rewritten in the following form:

$$\frac{dp_i(t)}{dt} = \alpha_V[1 - p_i(t)] - \alpha_{SV}p_i(t) + \beta a^2 \frac{[p_{i+1}(t) + p_{i-1}(t) - 2p_i(t)]}{a^2} \quad (58)$$

The latter part of Eq. (58) is a discrete analogy of the second-order spatial derivative. Hence, using the continuous coordinate $x \approx ia$, we obtain the following second-order partial differential equation instead of Eq. (58):

$$\frac{\partial p}{\partial t} = \alpha_V(1 - p) - \alpha_{SV}p + D\frac{\partial^2 p(t,x)}{\partial x^2} \quad (59)$$

where $p(t, x)$ is the probability of the occurrence of an overturned molecule at time $t$ at point $x$ and $D=\beta a^2$ is the effective diffusion coefficient of the molecule-overturned state along the surface. The extension of Eq. (59) to the plane (two-dimensional) case of further interest is, as was stated before, a straightforward procedure: it is reduced to the simple substitution of the partial second-order derivative with respect to one coordinate $x$ for the sum of the partial second-order derivatives with respect to $x$ and $y$ because in the two-dimensional case, $p=p(t, x, y)$.

According to the previous consideration, the transfer of the overturned state is determined only by the interactions between adjacent molecules and should vanish in two cases: (i) in the absence of interactions between adjacent amphiphilic molecules, i.e., at $\chi=0$ (in this case, $\beta=0$ and hence $D=0$); (ii) upon unlimited increase in the distance $a$ between adjacent molecules, i.e., when the surface concentration of molecules capable of overturning tends to zero; in this case, interactions between adjacent molecules also vanishes. Indeed, if $U_{th}$, $U_{tt}$, and $U_{hh}$ are determined by dispersion interactions, then $\chi(a)\sim B/a^6$, where $B$ is a constant expressed via the polarizabilities of hydrophilic head groups and hydrophobic tails: $B=(2A_{th}-A_{tt}-A_{hh})z/3$, where $A_{th}$, $A_{tt}$, and $A_{hh}$ are the corresponding Hamaker constants. Consequently, $D(a)\sim\beta[\exp B/a^6-1]a^2\sim\beta B/a^4\to 0$ with an increase in distance $a$ between adjacent amphiphilic molecules.

In the equilibrium state, the probability $p$ does not depend either on time or coordinate; this equilibrium state is further denoted by $p_v$, which is readily determined from Eq. (59):

$$p_V = \frac{\alpha_V}{\alpha_V + \alpha_{SV}} = \frac{1}{1 + \alpha_{SV}/\alpha_V} \quad (60)$$

From definitions (54) and (55), we obtain that $\frac{\alpha_{SV}}{\alpha_V} = \exp(2\Re_V) \gg 1$, i.e., $p_v$ is a small value.

The similar consideration to those used for derivation of Eq (59) results in the case of the events occurring underneath the aqueous droplet at the solid–water interface in the following equation:

$$\frac{\partial p}{\partial t} = \alpha_W(1 - p) - \alpha_{SW}p + D\frac{\partial^2 p(t,x)}{\partial x^2} \quad (61)$$

where subscript W refers to water; corresponding constants, $\alpha_W$ and $\alpha_{SW}$, can be obtained from (54)–(56) by substituting subscript W instead of V. The equilibrium value of the probability of the occurrence of an amphiphilic molecule in the overturned state

$$p_W = \frac{\alpha_W}{\alpha_W + \alpha_{SW}} \quad (62)$$

is determined, as in the case of contact with the air, from Eq. (61). Unlike the case of contact with the air, the $p_W$ probability is not a small value; on the contrary, it is close to one. It is this difference in probabilities that provides for the possibility of the aqueous droplet spreading over the initially hydrophobic surface.

Note that in the absence of lateral interactions between adjacent amphiphilic molecules, the aqueous droplet may not spread over the surface under consideration despite the effect of overturning of molecules with the hydrophilic portions upward, underneath the water. Indeed, let, in the absence of interactions between adjacent molecules, the necessary quantity of molecules be overturned with their hydrophilic portions upward (upper part in Fig. 20), and the substrate surface underneath the aqueous droplet becomes sufficiently hydrophilic so that the droplet edge can move into the adjacent position (lower part in Fig. 20). However, in the absence of lateral transfer of the overturned state of the amphiphilic molecules in the substrate, the surface both in front of the droplet edge in position 2 and behind the edge are still in the initial hydrophobic state, thus forcing the droplet edge to return immediately to the initial position 1. Thus, if the diffusion terms in Eqs. (59) and (61) vanish in the absence of the lateral transfer of the overturned state,

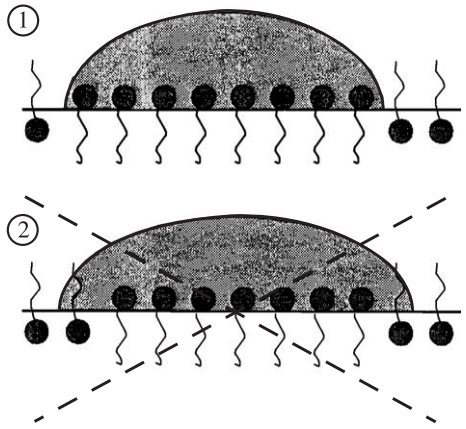


Fig. 20. Impossibility of a spreading of a water droplet on a hydrophobic substrate without lateral interaction between neighbouring chains (explanation in the text).

then the spreading of the aqueous droplet over the surface becomes impossible (Fig. 20)). However, if the adjacent amphiphilic molecules interact with each other and the lateral transfer of the overturned state due to these interactions is possible, the droplet edge moves over the surface and this motion is determined exactly by the rate of the lateral transfer of the overturned state of the substrate molecules.

### 6.2. Boundary conditions

According to the theory described above, the propagation of the overturned state of amphiphilic molecules along the surface under the droplet is described by Eq. (59) and the propagation beyond the droplet by Eq. (61). It is required now to formulate the boundary conditions for the $p(t, r)$ value at the boundary of the spreading axisymmetric droplet, i.e., at $r=r(t)$ (Fig. 21).

In view of the assumption of the absence of evaporation, the droplet volume $V$ remains constant during the spreading and it is assumed also that the droplet is small enough, that is, the gravity action may be neglected. The time scale of the spreading process is so low (see below) that the deformations of the drop profile caused by the spreading can be neglected. The latter means that the droplet retains the shape of a spherical segment during the spreading and described by Eq. (51).

Let us denote surface (interfacial) tensions for the water–air (constant value), substrate–air, and substrate–water interfaces directly at the boundary of the spreading droplet by $\gamma$, $\gamma_{SV}(t)$, and $\gamma_{SW}(t)$, respectively. Note that the values of $\gamma_{SV}(t)$ and $\gamma_{SW}(t)$ near the droplet edge differ from the constant values of surface tensions at the polymer–air and polymer–water interfaces far from the edge of the spreading droplet and in the depth of the droplet, respectively. It is assumed that the Young condition (quasi-equilibrium spreading) is satisfied at any moment at the boundary of the spreading droplet

$$\cos\theta = \frac{\gamma_{SV}(t) - \gamma_{SW}(t)}{\gamma} = \cos\theta^0 + \Delta(t) \tag{63}$$

$$\cos\theta^0 = \frac{\gamma^0_{SV} - \gamma^0_{SW}}{\gamma}\,\Delta(t) = \frac{\gamma_{SV}(t) - \gamma^0_{SV}}{\gamma} - \frac{\gamma_{SW}(t) - \gamma^0_{SW}}{\gamma}$$

In the latter equation, superscript 0 marks corresponding initial values of interfacial tensions. Note that the $\Delta(t)$ value is positive and increases with time because the $\gamma_{SV}(t)$ value increases with time due to possible appearance of hydrophilic head groups of the amphiphilic molecules at the substrate surface; in contrast, the $\gamma_{SW}(t)$ value decreases with time due to overturning of molecules under the droplet.

Let us emphasize once more:

(i) In view of the lateral interaction between adjacent amphiphilic molecules of the substrate, the overturned state may be extended beyond the boundary of the spreading droplet, resulting in an increase in surface tension of the substrate $\gamma_{SV}(t)$ in front of the moving droplet;

(ii) Interfacial tensions $\gamma_{SV}(t)$ and $\gamma_{SW}(t)$ do not remain constant near the droplet boundary but vary depending on the coordinate in a close vicinity of the boundary of the moving droplet (see below). Hence, interfacial tensions in the close vicinity of the edge of the moving droplet or, in a more formal manner, the limiting values of these tensions at $r \to r(t)$ from the inner and outer droplet sides enter the Young Eq. (63).

Corresponding limits of the degree of overturning inside and outside the droplet are denoted by $p_{in}$ and $p_{out}$, respectively (Fig. 21). Evidently, the $\Delta(t)$ value is not an explicit function of time but depends on time in an implicit manner via the values of $p_{in}$ and $p_{out}$, i.e., $\Delta=\Delta(p_{in}, p_{out})$. As it is shown below, in view of the equality of chemical potentials of amphiphilic molecules between the inner and outer boundaries of a droplet, the $p_{out}$ value is expressed as a function of $p_{in}$. Hence, in view of the latter dependence, actually $\Delta=\Delta(p_{in})$.

Let us use an Antonov's rule to determine unknown dependence $\Delta(p_{in}, p_{out})$, which means the additivity of the formation of the interfacial tensions.

Let $\gamma^{\infty}_{SW}$ and $\gamma^{0}_{SW}$ be the interfacial tensions under the droplet in the case when all molecules are overturned (all hydrophilic head groups are oriented upward) and when neither of these molecules is overturned (all hydrophilic head groups are oriented downward), respectively. Similar surface tensions outside the droplet are denoted by $\gamma^{\infty}_{SV}$ and $\gamma^{0}_{SV}$, respectively. According to the assumption of the

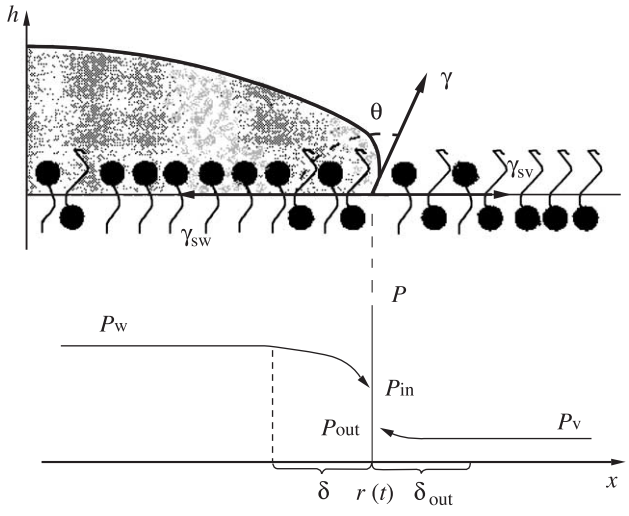


Fig. 21. Spreading of a spherical droplet: $r_o(t)$—radius of the basis of a drop, $\theta(t)$—dynamic contact angle, $h$—height at center of a drop.

additivity, the interfacial tensions in the closest vicinity of a droplet acquire the following form:

$$\gamma_{SV} = \gamma^0_{SV}(1 - p_{out}) + \gamma^\infty_{SV} p_{out},$$
$$\gamma_{SW} = \gamma^0_{SW}(1 - p_{in}) + \gamma^\infty_{SW} p_{in} \quad (64)$$

Substitution of relationships (64) into the Young Eq. (63) yields the following expression for the dependence $\Delta(p_{in}, p_{out})$ under consideration:

$$\Delta(p_{in}, p_{out}) = \frac{\gamma^\infty_{SV} - \gamma^0_{SV}}{\gamma} p_{out} + \frac{\gamma^0_{SW} - \gamma^\infty_{SW}}{\gamma} p_{in} \quad (65)$$

The obtained dependence, $\Delta(p_{in}, p_{out})$, is a linear function with respect to both variables.

As it is mentioned above, the spreading process under consideration is very slow (the time scale is hours). Because of this, below, we employ the principle of local equilibrium accepted in nonequilibrium thermodynamics. In accordance with this principle, chemical potentials of overturned and non-overturned amphiphilic molecules remain equal from both sides of the droplet boundary, i.e.,

$$\mu(p_{in}, \chi) = \mu(p_{out}, \chi) + \Im, \quad \Im = \frac{U_{hv} - U_{hw}}{RT} \quad (66)$$

The $\mu(p,\chi)$ dependence may be given, for example, in accordance with the Flory–Huggins theory in the following form: $\mu(p, \chi)=\ln p+\chi(1-p)^2$ [20]. We will not specify this dependence below but consider only two limiting cases of weak and strong lateral interactions between amphiphilic molecules. At this stage, it is enough to assume that, according to the equality of chemical potentials (66), $p_{out}$ and $p_{in}$ are interrelated by the known dependence $p_{out}=\varphi(p_{in})$. In view of all that has been said above, the value of $\Delta$ is dependent on only one variable, i.e., $\Delta=\Delta(p_{in})$.

In view of the equality $\tan\frac{\theta}{2} = \left(\frac{1-\cos\theta}{1+\cos\theta}\right)^{1/2}$ from Eq. (51), we obtain

$$r(p_{in}) = \left(\frac{6V}{\pi}\right)^{1/3} G(p_{in}), \quad (67)$$

where

$$G(p_{in}) = \frac{1}{\left(\frac{1-A}{1+A}\right)^{1/6}\left(3 + \frac{1-A}{1+A}\right)^{1/3}},$$
$$A(p_{in}) = \cos\theta^0 + \Delta(p_{in}) \quad (68)$$

Eq. (67) allows determining the final droplet radius, $r_\infty$, at the end of the spreading process using the known dependence $G(p_{in})$; to this end, it is necessary to substitute the expression for the equilibrium fraction of overturned molecules under droplet $p_W$ from relationship (62) into Eq. (67), which yields

$$r_\infty = \left(\frac{6V}{\pi}\right)^{1/3} G(p_W) \quad (69)$$

It is easy to verify that $G(p)$ is an increasing function of $p$, i.e., $r(t)$ increases, approaching its final value determined by Eq. (69).

Let us consider now the formulation of boundary conditions on a moving droplet edge. Two boundary conditions are required because the edge itself moves and the law of this movement should be determined.

The first boundary condition expresses the balance of the number of overturned molecules at the boundary of the moving droplet, and it has the following form:

$$-D\left.\frac{\partial p}{\partial r}\right|_{r=r(t)-} + D\left.\frac{\partial p}{\partial r}\right|_{r=r(t)+} = (p_{in} - p_{out})\frac{dr(t)}{dt} \quad (70)$$

As it is mentioned earlier, it is necessary to set the second boundary condition relating the $p_{in}$ and $p_{out}$ values because the other boundary conditions are straightforward: the symmetry in the droplet center, i.e.,

$$\left.\frac{\partial p}{\partial r}\right|_0 = 0 \quad (71)$$

and the tendency of the fraction of overturned molecules far from the droplet to the equilibrium value at the substrate–air interface that is determined from Eq. (59) as

$$p \rightarrow p_V. \quad (72)$$

We use below the condition of equality of chemical potentials of overturned molecules to the right- and left-hand sides of the moving boundary of a droplet [$r=r(t)$], which determines the dependence

$$P_{out} = \varphi(P_{in}) \quad (73)$$

To analyze the dependences of chemical potentials, we employ the expressions resulting from the Flory–Huggins theory [20] modified to take into account the interactions of amphiphilic molecules with the environment and the underlying molecules of a substrate, namely, interactions of their hydrophilic head groups with water and their hydrophobic tails with the substrate molecules (under the droplet) and interactions of hydrophilic head groups with the air and hydrophobic tails with underlying substrate molecules (outside the droplet). This leads to the following expression:

$$\ln p_{in} + \chi(1 - p_{in})^2 = \ln p_{out} + \chi(1 - p_{out})^2 + \Im \quad (74)$$

where $\chi$ is the known parameter of interaction of amphiphilic molecules with each other; in this case, the value of $z$ is equal to 4 [see expression below Eq (56)].

In the case of weak interactions between adjacent molecules, i.e., at $\chi \ll \Im$, from expression (74), we have ln

$p_{in}$=ln $p_{out}$+$\Im$. As a result, we have the Boltzmann's distribution:

$$p_{out} = p_{in}\exp(-\Im) \tag{75}$$

In the case of strong interaction between the neighbouring molecules, i.e., $\chi \gg \Im$, we obtain

$$\ln p_{in} + \chi(1-p_{in})^2 = \ln p_{out} + \chi(1-p_{out})^2 \tag{76}$$

Hence, it results in equality of overturned fractions: $p_{out}$=$p_{in}$.

The value of $p_{out}$ is always smaller than or equal to $p_{in}$, thus enabling us to solve Eq. (66) for the arbitrary case and to express $p_{out}$ as a function of $p_{in}$ which was stated before.

Thus, the problem of droplet spreading acquires the following form: the dependence $p(t, r)$ under the droplet [$0<r<r(t)$] is described by the equation

$$\frac{\partial p}{\partial t} = \alpha_W(1-p) - \alpha_{SW}p + D\frac{1}{r}\frac{\partial}{\partial r}r\frac{\partial p}{\partial r} \tag{77}$$

and the dependence $p(t, r)$ outside the droplet, $r>r(t)$, is described by the equation

$$\frac{\partial p}{\partial t} = \alpha_V(1-p) - \alpha_{SV}p + D\frac{1}{r}\frac{\partial}{\partial r}r\frac{\partial p}{\partial r} \tag{78}$$

with the following boundary conditions: condition of symmetry in the droplet center [Eq. (71)], condition (72) far from the droplet, condition (67) expressing the radius of the spreading droplet via $p_{in}$, condition (70) expressing the equality of fluxes at the moving boundary of the droplet $r=r(t)$, and relationship (66) expressing the equality of chemical potentials of overturned molecules near the moving edge of the droplet.

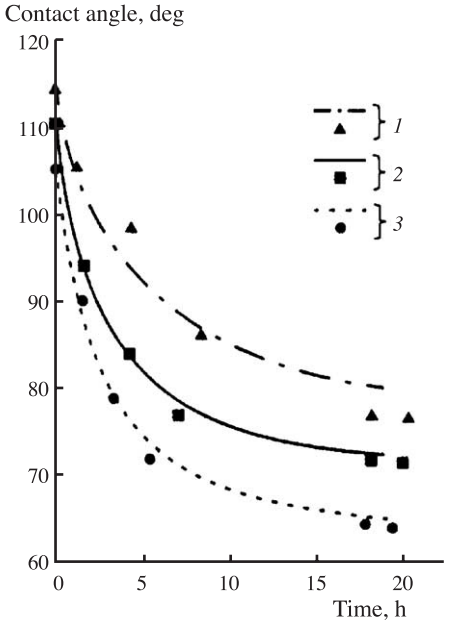


Fig. 22. Time dependences of contact angle, $\theta$, of water droplets at the surface of paraffin containing stearic acid of different concentrations in wt.% (experimental data from Ref. [17]): $C$=0.6, $C$=2.0, $C$=9.0. Solid lines calculated according to Eq. (79) using $t^*$ as a fitting parameter.

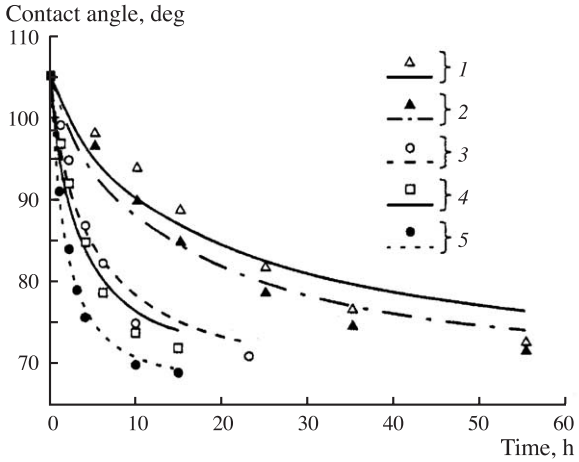


Fig. 23. Time dependences of the contact angle, $\theta$, of water droplets at the surface of a Langmuir–Blodget films formed by a stearic acid at various temperatures in °C: Experimental data from Ref. [18]. $t^*$=13.5 h, $t^*$=15.5 h, $t^*$=23.0 h, $t^*$=25.0 h, $t^*$=28.5 h. Solid lines calculated according to Eq. (79) using $t^*$ as a fitting parameter.

### 6.3. Solution of the formulated problem

We perform the solution of the formulated problem introducing a number of simplifying assumptions whose validity is checked in Ref. [19].

- Under the main part of the droplet, the value of $p$ is independent of the coordinate and equal to its equilibrium value Eq. (62); the same is true outside the droplet: $p$ differs from its equilibrium value Eq. (60) only in a narrow region close to the droplet edge.

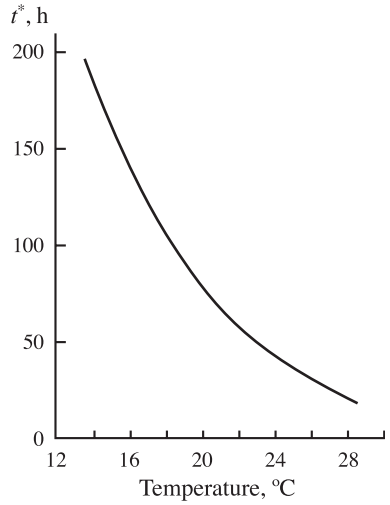


Fig. 24. Dependence of characteristic time of a spreading of drops, $t^*$, on temperature.

- The latter means that probability, $p$, differs from its equilibrium values in narrow regions, $\delta$ and $\delta_{out}$, under and outside the droplet, respectively (Fig. 21).

$$\frac{dp_{in}}{dt} = \frac{(1-p_{in})/t^*}{G'(p_{in})\sqrt{p_{in}}} \quad (79)$$

where $\delta = \sqrt{D/(\alpha_W + \alpha_{SW})}, t^* = r^*\delta/D, r^* = (6V/\pi)^{1/3}$.

Thus, according to the proposed theory, the droplet spreads in a completely different manner than was suggested in Refs. [17,18], i.e., the equilibrium concentration of overturned amphiphi1ic molecules (or their fragments) is established rapidly (as compared to the characteristic time of spreading) under the main portion of the drop and retains its value over the course of the entire spreading process. All changes occur only within the narrow region in the vicinity of the perimeter of the spreading droplet.

### 6.4. Comparison between theory and experimental data

Eq. (79) contains one unknown parameter, $t^*$, which is the characteristic time of the propagation of the overturned state, i.e., the characteristic time of droplet spreading. Parameter $t^*$ was used as an adjustment parameter for the comparison of the theoretical predictions according to the above theory and experimental data reported elsewhere [17, 18].

In Fig. 22, the time dependences of the contact angle of an aqueous droplet at the surface of paraffin containing steric acid at various concentrations, $C$, are presented. Lines show the solutions of Eq. (79) and the symbols denote experimental data [18] for three different concentrations, $C$. The values of $t^*$ were found as follows:

$t^*$=50.5 h at $C$=0.6 wt.%,
$t^*$=27.5 h at $C$=2.0 wt.%,
$t^*$=24.0 h at $C$=9.0 wt.%.

The latter values show that as the concentration of stearic acid increases, the characteristic time of propagation of the overturned state decreases. The latter is due to an increase in "diffusion coefficient" $D$ because of the decreasing average distance between acid molecules capable of overturning.

In Fig. 23, the time dependences of the contact angle of aqueous drops at a Langmuir–Blodgett films composed of stearic acid at various temperatures are presented. Here, symbols represent experimental data from Ref. [17] and lines drawn correspond to the solutions of Eq. (79). The deduced dependence of parameter $t^*$ on temperature is shown in Fig. 24. Characteristic time $t^*$ of the propagation of the overturned state decreases with temperature, which may be explained by an increase in the rotational mobility of molecules capable of overturning and simultaneously the "diffusion coefficient" $D$ of the overturned state of stearic acid molecules increases.

## Acknowledgement

The author acknowledges the contributions made by the co-workers and the financial support by the Royal Society, UK (grant 15544).

## References

[1] V.M. Starov, S.R. Kosvintsev, V.D. Sobolev, M.G. Velarde, S.A. Zhdanov, J. Colloid Interface Sci. 252 (2002) 397.
[2] V.M. Starov, S.A. Zhdanov, M.G. Velarde, S.R. Kosvintsev, V.D. Sobolev, Adv. Colloid Interface Sci. 104 (2003) 123–158.
[3] V.M. Starov, S.R. Kosvintsev, V.D. Sobolev, M.G. Velarde, S.A. Zhdanov, J. Colloid Interface Sci. 246 (2) (2002) 372.
[4] V. Starov, V. Zhdanov, Colloids Surf., A Physicochem. Eng. Asp. 192 (2001) 363.
[5] S. Zhdanov, V. Starov, V. Sobolev, M. Velarde, Spreading of aqueous SDS solutions over nitrocellulose membranes, J. Colloid Interface Sci. 264 (2003) 481–489.
[6] N.V. Churaev, G.A. Martynov, V.M. Starov, Z.M. Zorin, Colloid Polym. Sci. 259 (1981) 747.
[7] V.J. Starov, Colloid Interface Sci. 270 (2003) 180.
[8] V.M. Starov, A. de Ryck, M.G. Velarde, J. Colloid Interface Sci. 190 (1997) 104.
[9] V. Starov, S. Zhdanov, M. Velarde, J. Colloid Interface Sci. 273 (2004) 589.
[10] V.M. Starov, S.R. Kosvintsev, M.G. Velarde, J. Colloid Interface Sci. 227 (2000) 185.
[11] J.D. Andrade, W.-Y. Chen, Surf. Interface Anal. 8 (6) (1986) 253.
[12] J.D. Andrade (Ed.), Polymer Surface Dynamics, Plenum, New York, 1988.
[13] B.K. Lewis, B.D. Ratner, J. Colloid Interface Sci. 159 (1) (1993) 77.
[14] M. Miyama, Y. Yang, T. Yasuda, et al., Langmuir 13 (20) (1997) 5494.
[15] V.M. Rudoy, S.D. Stuchebryukov, V.A. Ogarev, Colloid J. Russ. Acad. Sci. 50 (1) (1988) 199 (English Translation).
[16] I. Langmuir, Science 87 (1938) 493.
[17] P.N. Yiannos, J. Colloid Sci. 17 (4) (1962) 334.
[18] E. Rideal, J. Tadayon, Proc. Roy. Soc. (London) A 225 (1162) (1954) 346.
[19] V.M. Starov, V.M. Rudoy, V.I. Ivanov, Colloid J. (Russian Academy of Sciences English Translation) 61 (3) (1999) 374.
[20] P.J. Flory, Principles of Polymer Chemistry, Cornell Univ. Press, Ithaca, 1990.